Imminent loss of climate space for permafrost peatlands in Europe and Western Siberia

Richard E. Fewster[a]*, Paul J. Morris[a], Ruza F. Ivanovic[b], Graeme T. Swindles[c,d], Anna Peregon[e,f], and Christopher J. Smith[b,g]

[a]*School of Geography, University of Leeds, Leeds, United Kingdom, LS2 9JT*
[b]*School of Earth and Environment, University of Leeds, Leeds, United Kingdom, LS2 9JT*
[c]*Geography, School of Natural and Built Environment, Queen's University Belfast, Belfast, United Kingdom, BT7 1NN*
[d]*Ottawa-Carleton Geoscience Centre and Department of Earth Sciences, Carleton University, Ottawa, Ontario, Canada*
[e]*Institute of Soil Science and Agrochemistry (ISSA), Siberian Branch of the Russian Academy of Sciences (SB RAS), Pr. Akademika Lavrentyeva, 8/2, 630090, Novosibirsk, Russian Federation*
[f]*Tuvan State University, Republic of Tuva, Lenina St., 36, Kyzyl, 667000, Russian Federation*
[g]*International Institute for Applied Systems Analysis (IIASA), A-2361 Laxenburg, Austria*

** Corresponding author, Email address:* gy15ref@leeds.ac.uk *(*R.E. Fewster*)*

Human-induced climate warming by 2100 is expected to thaw large expanses of northern permafrost peatlands. However, the spatio-temporal dynamics of permafrost peatland thaw remain uncertain due to complex permafrost-climate interactions, the insulating properties of peat soils, and variation in model projections of future climate. Here we show that permafrost peatlands in Europe and Western Siberia will soon surpass a climatic tipping point under scenarios of moderate-to-high warming (SSP2-4.5, SSP3-7.0, and SSP5-8.5). The total peatland area affected under these scenarios contains 37.0–39.5 Gt carbon (equivalent to twice the amount of carbon stored in European forests). Our bioclimatic models indicate that all of Fennoscandia will become climatically unsuitable for peatland permafrost by 2040. Strong action to reduce emissions (SSP1-2.6) by the 2090s could retain suitable climates for permafrost peatlands storing 13.9 Gt carbon in northernmost Western Siberia, indicating that socioeconomic policies will determine the rate and extent of permafrost peatland thaw.

Main

Permafrost peatlands represent ~45 % (185 Gt) of the soil organic carbon (SOC) stored in northern peatlands[1] and are particularly threatened by rapid 21st century climate change across the Arctic[2]. Thawing of peatland permafrost enhances CO_2 emissions[3], while waterlogging from surface collapse can increase CH_4 emissions[4]. Peatland permafrost responds differently to changing climates than mineral-soil permafrost, due to the insulating properties of organic soils[5], but peatlands remain poorly represented in Earth system models[1]. Some dynamic global vegetation models (DGVMs) have approximated permafrost distribution in peatlands using simulated soil temperatures[6,7], but do not distinguish different permafrost forms (e.g. ice lenses or ice wedges) or their differing relationships with climate. Modelling of permafrost-temperature relationships has predicted that a warming of 2°C above preindustrial climates would thaw 700,000 km^2 of peatland permafrost along its southern limit, which would shift northern peatlands from a net carbon sink to a net carbon source[1]. However, the timing of such changes is highly uncertain. Furthermore, snow cover and summer rainfall are known to play important roles in determining the distribution of peatland permafrost[8,9], meaning future changes to precipitation regimes must also be considered. The latest generation of global climate models (CMIP6) project substantially warmer climates by 2100 than previous generations (e.g. CMIP5)[10,11], raising the pressing question of how these new projections may impact estimates of 21st century permafrost peatland thaw.

Peatland permafrost distributions can be mapped from the presence of characteristic landforms. Peat-covered frost mounds, termed palsas or peat plateaus depending on their spatial extent[12], are formed through the frost heaving of segregated ice lenses and predominantly exist in regions of discontinuous permafrost[8]. Further north, where permafrost is continuous, ice-wedge polygons form where extreme winter temperatures cause thermal cracking of peatland surfaces[13,14]. Modern permafrost peatland distributions are well-constrained in Fennoscandia[15,16] and Western Siberia[17,18], but observations from North America are more sporadic[19,20] and are absent across much of central and eastern Siberia. We may expect these distinct ice forms, and their carbon stocks, to exhibit different responses to climate, yet large-scale, forward-looking simulations have never compared them.

Bioclimatic models fitted specifically to palsa/peat plateau distributions in Fennoscandia[15,16,21,22] and North America[20] suggest that these landforms occupy narrow climate envelopes of cold, dry conditions. Such models have suggested that a 1°C temperature increase could halve the present palsa extent in Fennoscandia, and that medium to high anthropogenic emissions could render the entire region climatically unsuitable for palsas by 2070–2099[15]. Future modelling of ice-wedge polygons, including those from non-peat soils, suggest that these ice forms are supported by intensely cold environments with < 300 mm yr^{-1} rainfall: an envelope that could halve by 2061–2080 under very high emissions[9].

Anthropogenic climate change is expected to cause widespread thawing of permafrost peatlands[1,6,15]. The increased warming projected by CMIP6 models suggests that previous studies may have underestimated the extent of near-future permafrost peatland degradation. Climate envelope models are powerful tools for understanding permafrost peatland responses to changing climate[9,15,20,22], but such models have not yet been fitted to palsas, peat plateaus and polygon mires in Western Siberia. Here, we determine the changing climate envelopes of permafrost peatlands in Europe and Western Siberia during the 21st century, and estimate the associated risk for peat carbon stocks. To achieve this, we compiled a new dataset of permafrost peatland landforms and developed bioclimatic models which were driven by CMIP6 climate projections. We then compared our simulations to a peat carbon map[1], to identify peatlands at risk under future climate change.

We used one-vs-all logistic regression modelling to establish the modern baseline (1961–1990) climate envelopes that support palsas/peat plateaus and polygon mires in Europe and Western Siberia. We drove these bioclimate models using future climate projections from the Coupled Model Intercomparison Project phase 6 (CMIP6)[23] for each decade from the 2020s to the 2090s, to estimate likely spatiotemporal changes in permafrost peatland climate envelopes. We combined our bioclimate projections with a map of peatland SOC[1], as a measure of the risk associated with shrinking climate envelopes. CMIP6 represents the latest generation of general circulation and Earth system models, many of which provide higher estimates of climate sensitivity than previous CMIP generations[10,11]. We selected an ensemble of 12 independent CMIP6 models (i.e. without shared components or a common origin)[24] (see

methods). Our CMIP6 ensemble has an equilibrium climate sensitivity range of 1.9–4.8°C (median of 3.0°C) (Table S1). To produce 21st century climate projections, CMIP6 models were driven by Shared Socioeconomic Pathways (SSPs), a range of scenarios that span potential future societal developments and anthropogenic emissions[25]. We selected four scenarios for analysis: SSP1-2.6 (strong climate change mitigation), SSP2-4.5 (moderate mitigation), SSP3-7.0 (no mitigation baseline) and SSP5-8.5 (no mitigation, worst-case).

Modern climate envelopes of permafrost peatlands

Our study presents a newly compiled, binary, 0.5° × 0.5° spatially-gridded catalogue of observed permafrost peatland landforms across the northern hemisphere, with 885 grid cells containing observed palsas/peat plateaus and 510 grid cells containing observed polygon mires (Supplementary datasets S1 and S2). The majority (71 %) of gridded observations were concentrated in Europe and Western Siberia, between 25°W and 95°E (Figure S1). By comparison, the low density of observations in Canada, Alaska, and central and eastern Siberia suggests that the true distribution of landforms in these regions is underestimated by published records. We therefore focused on regional predictions for Europe and Western Siberia, where we have greatest confidence in the modern observed distribution of permafrost peatlands (see methods for details on the study domain).

Our climate envelope models for Europe and Western Siberia (Tables S2 and S3) showed predictive accuracies of 94 % for palsas/peat plateaus, and 96 % for polygon mires (Table S4), indicating that climate is the primary control of permafrost peatlands at broad spatial scales[9,16,20,21]. Our models slightly overpredict the southern extent of observed permafrost peatland landforms (Figure 1a,b), which suggests that our projections of future climate space likely represent an upper limit. Our results indicate that cold, dry climates are optimal for palsa/peat plateau persistence in Europe and Western Siberia (spatial medians of 30-year mean annual temperature (*MAT*) = -4.7°C; and mean annual rainfall = 283 mm yr^{-1}) (Table S5). Palsas in Fennoscandia were previously identified alongside an average MAT of -2.6°C–-2.4°C during 1961–1990[16,21], which suggests that Fennoscandian palsas exist under warmer climates than elsewhere, for example those in Western Siberia. Polygon mires require even colder temperatures (*MAT* = -8.3°C) and < 300 mm yr^{-1} of snowfall, which agrees with previous

pan-Arctic modelling[9]. We estimate that 1.14 million km^2 of Europe and Western Siberia, and 34.4 Gt peat C, existed within the suitable climate envelope for palsas/peat plateaus during the modern baseline period (1961–1990); whilst 591,000 km^2, and 15.3 Gt peat C, existed within the suitable climate envelope for polygon mires (Figure 1).

Climate space loss under the strongest mitigation scenario

SSP1-2.6 represents a low emissions pathway with strong climate mitigation policies, where global net CO_2 emissions become negative after 2075. Radiative forcing peaks and begins to decline during the late 21st century[10], reaching 2.6 W m^{-2} by 2100[25]. Our CMIP6 model ensemble projects an inter-model median change in *MAT* from the modern baseline period (1961–1990) of +2.8°C (interquartile range (IQR) = 1.7–3.1°C) during the 2090s under SSP1-2.6 for peatlands of Europe and Western Siberia, compared to +2.0°C (IQR = 1.7–2.5°C) globally (Table 1). Previous projections of peatland permafrost thaw under +0.5°C to +2.0°C equilibrium warming scenarios[1,15,26] therefore underestimate the levels of warming that our estimates project for the late 21st century. Where climates do become unsuitable, the insulating properties of peat soils could allow relict peatland permafrost to endure for some time, although new permafrost would no longer develop[27,28].

Under SSP1-2.6, our simulations suggest that between 1961–1990 and 2020–2029 the suitable climate envelope for palsas/peat plateaus will have contracted by 38 % or 431,000 km^2 (Figures S3–S4). During this period, our modelling projects the envelope in Fennoscandia to have contracted by 89 % (129,000 km^2). Late 21st century cooling following a mid-century temperature peak under SSP1-2.6 will not be sufficient to re-establish suitable climatic conditions in Fennoscandia. Given the comparatively low levels of warming presented by SSP1-2.6 (Table 1), this suggests that permafrost peatlands in Fennoscandia are close to, or may have already passed, a climatic tipping point. It therefore seems possible that large areas of the suitable climate space seen in the baseline period may have already been lost. Published observations indicate that palsa/peat plateau thaw has occurred throughout the late 20th century in Fennoscandia[29], with degradation accelerating at several sites from the mid-1990s[30,31]. Our estimates show permafrost peatlands in Fennoscandia contain substantially less SOC (1.5 Gt C) than those in Western Siberia (35.9 Gt C), but widespread

thaw could also cause extensive inundation[4,32], habitat and vegetation shifts[33,34], and release of dissolved organic carbon[35,36] and heavy metals[37] into aquatic systems. Ongoing ecological and hydrological changes in Fennoscandian peatlands over the coming decades will provide important early indications of likely ecosystem trajectories elsewhere across the pan-Arctic.

Our modelling projects mean losses of the palsa/peat plateau climate envelope under SSP1-2.6 of 70,000 km^2 per decade from the 2030s to the 2070s, reaching a minimum extent of 357,000 km^2 by the 2070s (Figures S3–S4). Unlike in Fennoscandia, a partial climatic recovery in Western Siberia by the 2090s is projected to return the climatically suitable area there to 563,000 km^2, with 257,000 km^2 located further north than during 1961–1990 (Figure 2), covering a region currently characterised by polygon mires[13,17]. However, this median projected area is less certain than some of our other predictions because our CMIP6 12-model ensemble presents a wide range of projections for the 2090s under SSP1-2.6 (IQR = 508,000 km^2) (Figure S3).

By the 2090s, our simulations indicate that peatlands containing 24.9 Gt SOC will no longer exist within the suitable climate envelope for palsas/peat plateaus under SSP1-2.6. An additional 7.6 Gt SOC may be affected by the temporary contraction of the climate envelope, before a partial recovery beginning in the 2080s (Figure 3). The resilience of permafrost peatlands to temporary periods of climatic deterioration and recovery have rarely been considered. Observations from Finland have shown palsas completely thawing in less than 10 years[8,38], although frozen soils may persist longer where local environmental conditions offset unsuitable climates. For example, in central Canada some relict peatland permafrost has persisted since the Little Ice Age[27,39,40]. Once thawed, thermokarst ponds and changing vegetation may prevent permafrost from re-aggrading for several decades, even if suitable climates return[41,42].

Our results suggest that under SSP1-2.6 the suitable climate space for polygon mires in Western Siberia will contract to 99,000 km^2 by the 2070s, before recovering to 150,000 km^2 by the 2090s. The minimum extent reached by the 2070s represents an 83 % reduction in the modern climate envelope and would cause peatlands containing 13.7 Gt SOC to no longer exist under suitable climate conditions for ice-wedge polygons. From the 2040s, however, the Yamal and Gyda peninsulas are predicted to fall within the northwards-moving climate

envelope for palsas/peat plateaus, suggesting that new permafrost peatland landforms may begin to develop where suitable peat depths and *Sphagnum* moss communities exist[20,43]. The exact duration of palsa formation remains uncertain, but field experiments have observed nascent palsas developing after three years of snow clearances[8,44]. Considering palsas/peat plateaus and polygon mires together, the climatic recovery projected for the 2090s under SSP1-2.6 would provide suitable climates for permafrost peatlands across 599,000 km^2, a 47 % reduction from 1961–1990. However, these suitable climate envelopes would exist further north than present, supporting Arctic peatlands that contain substantially less carbon than those at lower latitudes, because cold, dry climates have restricted plant productivity and peat accumulation rates there since the early-Holocene[45]. These envelopes would therefore only support a combined permafrost peatland carbon stock of 14.9 Gt, a 62 % reduction from 1961–1990 (Figure 3).

Future changes under uninterrupted warming

The scenarios SSP2-4.5, SSP3-7.0 and SSP5-8.5 represent medium, high and very high 21st century emissions scenarios, resulting in global radiative forcings by 2100 of 4.5, 7.0, and 8.5 W m^{-2}, respectively[25]. Overall, our CMIP6 climate model ensemble indicates that peatlands in Europe and Western Siberia will experience inter-model median *MAT* increases from the modern baseline period (1961–1990) to the 2090s of +4.0°C (SSP2-4.5; IQR = 3.3–4.2°C), +5.9°C (SSP3-7.0; IQR = 5.1–7.0°C), and +7.3°C (SSP5-8.5; IQR = 6.2–8.0°C), which are greater than the projected global increases (Table 1). Northern high latitudes are projected to warm more quickly than other regions due to Arctic amplification[47]. By the 2050s, projected increases in *MAT* under SSP5-8.5 in some northern parts of Western Siberia, currently characterised by polygon mires, will surpass even the worst-case scenarios (+5.5–6°C warming) considered by recent equilibrium-climate modelling of permafrost peatlands[1]. Our ensemble also projects considerable increases in growing degree days, with warming winters leading to large increases in annual rainfall by the 2090s (Tables S7 and S8).

Our simulations indicate areal losses of the suitable climate envelope for palsas/peat plateaus across Europe and Western Siberia by the 2060s of 75 % (SSP2-4.5), 81 % (SSP3-7.0), and 93 % (SSP5-8.5) (equivalent to 0.85, 0.92, and 1.05 million km^2 respectively) (Figures S5–S7). By

the 2090s, these projected losses have increased to 87 % (SSP2-4.5), 98 % (SSP3-7.0), and 100 % (SSP5-8.5) (equivalent to 0.99, 1.11, and 1.14 million km^2) (Figure 2) and the inter-model agreement is strong compared to SSP1-2.6 (Figure S3). Climate space is projected to contract most quickly before the 2070s. From the 2040s, suitable climates for palsas/peat plateaus are projected to be absent from Fennoscandia and persist only on the Yamal and Gyda peninsulas in Western Siberia, an area presently characterised by polygon mires[13,17]. However, continued warming under SSP3-7.0 and SSP5-8.5 would likely hinder any new palsa/peat plateau formation in these northernmost regions.

A shift towards warmer and wetter Arctic climates means that under continuous warming scenarios the modern climate envelope that supports polygon mires will have almost completely disappeared by the 2060s (with losses of 551,000–591,000 km^2, or 93–99.9 %, depending on scenario) (Figures S5–S7). By the 2090s, our simulations indicate that almost all of Europe and Western Siberia would be climatically unsuitable for permafrost peatlands under these scenarios, potentially leaving 37.0 (SSP2-4.5)–39.5 (SSP5-8.5) Gt of permafrost peatland carbon vulnerable to post-thaw decomposition (Figure 3). In comparison to SSP1-2.6, the combined suitable climate envelopes would support 12.1 (SSP2-4.5) to 14.9 (SSP5-8.5) Gt less permafrost peatland carbon by the 2090s, equivalent to 61–75 % of the total carbon stored in European forests[48].

We provide the first projections of the future climate spaces of polygon mires, and the first projections for palsas/peat plateaus in Western Siberia. Empirical modelling of ice-wedge polygons from all settings, including those formed in mineral soils, has suggested that some northern parts of Western Siberia could retain suitable climatic conditions during 2061–2080 under CMIP5's medium (RCP4.5) and very high (RCP8.5) warming scenarios[9]. Although this previous analysis demonstrated that ice-wedge distributions are primarily controlled by climate, these projections of suitable environmental space were also constrained by certain non-climatic predictors, including the availability of flat topography and coarse sediments[9]. Our modelling of broadly-equivalent CMIP6 scenarios indicates suitable climatic conditions for peatland polygons will exist only in the northernmost extremities of Western Siberia by the 2070s under medium warming (SSP2-4.5), and will be entirely absent from the region from the 2060s under very high warming (SSP5-8.5). Fennoscandia was previously projected to become climatically unsuitable for palsas during 2040–2069 under the CMIP2 scenario for

very high warming (A2)[15], but our CMIP6 modelling now indicates that widespread losses of climate space will occur imminently even under low warming (SSP1-2.6).

Post-thaw possibilities for peatland carbon

Once a climatic threshold is surpassed, the presence of thick peat soils and peatland vegetation are thought to delay permafrost thaw by maintaining cool ground temperatures[41,49]. Local-scale negative feedbacks such as this may allow some peatland permafrost to endure for a considerable time after climates become unsuitable[27]. The magnitude of this time lag in degradation varies between years[8] and decades[27,50], although observations suggest that thaw rates have accelerated under recent temperature increases[32,51]. Active-layer depths of certain palsas/peat plateaus in northern Sweden[30] and north-western Canada[52] have increased at rates of 2.3–3.3 cm yr^{-1} during recent decades. Indeed, the magnitude of 21st century climate change projected by our CMIP6 model ensemble (Tables 1, S6–S9) may be sufficient to overcome these feedbacks, rendering climate-induced thaw of permafrost peatlands unavoidable**.** For example, the rainfall increases projected for Fennoscandia could encourage seasonal inundation, which can lead to the complete thawing of palsas within a single year and prevent refreezing[8]. Future peatland permafrost thaw may occur more quickly under higher emission pathways, with our simulations showing twice as much warming in Western Siberia by the 2090s under SSP5-8.5 than under SSP2-4.5 (Table 1). We found no observational evidence of peatland permafrost persisting in Europe and Western Siberia under mean annual temperatures > 2.2°C during 1961–1990. However, under the SSP2-4.5, SSP3-7.0, and SSP5-8.5 scenarios only 29 %, 16 %, and 8 % of peat-containing grid cells are projected to remain below this *MAT* threshold by the 2090s.

Widespread thaw of northern permafrost peatlands will likely alter large-scale biosphere-atmosphere carbon fluxes, but the direction of the resulting radiative forcing remains an ongoing research question. On sub-decadal timescales, thaw of ice-rich palsas/peat plateaus and polygon mires often causes surface collapse and saturation as thermokarst ponds develop. Degrading permafrost peatlands can then transition into inundated Arctic fens[4], which commonly exhibit high CH_4 emissions[53]. If meltwaters drain away, enhanced aerobic

decomposition are likely to provoke large CO_2 emissions[54]. Under warming climates, woody vegetation is expected to expand northwards[55], increasing the susceptibility of northern peatlands to wildfire. Active layer depths in recently burned peatlands can be 30–90 cm deeper than in neighbouring unburned sites, which can greatly increase respiration of deep peat carbon[56,57], although such losses are inhibited by thermokarst[58]. Conversely, the projected onset of warmer, wetter climates would increase plant productivity in Arctic peatlands and eventually drive new surface peat accumulation, for example through terrestrialisation of thermokarst ponds[32,42], which could offset losses of deep peat carbon by 40 to > 100 %[59].

The expected simultaneous increases to peat decomposition and accumulation make it highly unlikely that entire peatland carbon stocks would be lost following thaw. Empirical modelling of post-thaw chronosequences suggests that deep peat carbon losses by respiration would occur rapidly (e.g. < 10 years), and would take several centuries to be replaced by new peat accumulation[1,60,61]. Modelled net carbon losses only exist for a small number of sites and vary widely (-35 to +2.7 kg C m^{-2} $century^{-1}$)[60,62], depending on relative timings of peat initiation and permafrost aggradation[59]. An analysis of five permafrost peatland chronosequences of varying permafrost histories from Alaska and north-western Canada has reported an average net carbon loss of 19 % during the first 100 years post-thaw[1,61], but similar analyses do not exist for peatlands in Europe or Western Siberia.

Previous hemispheric-scale modelling of CMIP5 simulations has suggested that northern peatlands will remain a weak carbon sink until the end of the 21st century[6,63,64], but these assessments should now be revised to incorporate the climate changes projected by CMIP6 ensembles. For example, DGVM simulations forced by CMIP6 climate projections indicate that northern peatlands will become net carbon sources by 2100, even under SSP1-2.6[7]. Here, our own CMIP6 modelling projects imminent, widespread losses of suitable climate space for permafrost peatlands in Europe and Western Siberia, which would have important implications for the future net carbon balance of northern peatlands.

Our modelling, which uses the latest generation of CMIP6 future climate projections, suggests that the suitable climate envelopes for palsas/peat plateaus and polygon mires in Europe and

Western Siberia are close to a tipping point. We project the widespread loss of climate space in Fennoscandia within the coming decade, and across the entire study region by 2100. Under the full range of future emission pathways, only 8,000–16,000 km^2 of Fennoscandia will retain climatically suitable conditions for palsas/peat plateaus by the 2030s, a reduction of 89–94 % compared to 1961–1990. In Western Siberia, even under the most optimistic climate scenario (SSP1-2.6) 93 % of current palsas/peat plateaus and 79 % of polygon mires will fall outside their suitable climate envelope by the 2070s, as both envelopes move northwards. Further warming projected by the 2090s under SSP3-7.0 and SSP5-8.5 would cause all of Europe and Western Siberia to become climatically unsuitable for peatland permafrost. Peatlands projected to no longer climatically support permafrost by the 2090s contain 24.9 (SSP1-2.6), 37.0 (SSP2-4.5), 39.2 (SSP3-7.0) and 39.5 (SSP5-8.5) Gt peat C. The onset of significantly warmer, wetter climates at these sites could accelerate permafrost thaw and exacerbate greenhouse gas emissions. However, probable increases in plant productivity and peat accumulation mean that the net effect upon radiative forcing warrants further investigation. SSP1-2.6, characterised by strict climate change mitigation, is the only scenario where our models project a partial recovery of the suitable climate envelope for palsas/peat plateaus by 2100.

Correspondence statement

Correspondence and requests for materials should be addressed to Richard Fewster (gy15ref@leeds.ac.uk).

Acknowledgements

R.E.F. is in receipt of a UK Natural Environment Research Council Training Grant (NE/S007458/1). A.P. is grateful for support of the Russian Science Foundation, grant 20-67-46018. The work of A.P. was carried out according to the State assignment of ISSA SB RAS. C.J.S. was supported by a NERC/IIASA Collaborative Research Fellowship (NE/T009381/1).

Author contributions

R.E.F., P.J.M., R.F.I., and G.T.S. designed the research. R.E.F. conducted the research and led manuscript development, with contributions from all authors. A.P. contributed landform classification data for Western Siberia. C.S. provided analysis of future climate projections from CMIP6 models.

Competing Interests

The authors declare no competing interests.

Tables

Table 1 – Projected regional mean annual temperatures for 2090–2099, with comparisons to the modern baseline period (1961–1990). Median projected, bias-corrected values of mean annual temperature (*MAT*) by 2090–2099; the change from the modern baseline period (1961–1990) (Δ *MAT*); and standard deviations of *MAT* across our CMIP6 model ensemble (Std. dev). *MAT* values were averaged across all grid cells that were classified to be climatically suitable for palsas/peat plateaus and polygon mires during the modern baseline period (Figure 2), for Fennoscandia and Russia. Our Russia region excludes the Kola Peninsula and Karelia, which are included in Fennoscandia. Antarctica is not included in CRU TS 4.04[46], so we exclude it from our global terrestrial average. For projected changes in other relevant climate predictors, see Tables S6–S9. For details on the bias-correction of climate variables, see methods.

Scenario	*MAT* (Δ *MAT*, Std. dev) (°C)			
	Palsas/peat plateaus in Fennoscandia	Palsas/peat plateaus in Russia	Polygon mires in Russia	Global land surface, excluding Antarctica
SSP1-2.6	-0.3 (+2.6, ±1.1)	-1.6 (+3.5, ±1.3)	-4.6 (+3.7, ±1.6)	11.0 (+2.0, ±0.6)
SSP2-4.5	1.1 (+4.0, ±1.0)	-0.4 (+4.7, ±1.2)	-3.0 (+5.2, ±1.5)	12.2 (+3.3, ±0.7)
SSP3-7.0	2.7 (+5.6, ±1.3)	2.2 (+7.3, ±1.7)	0.0 (+8.2, ±1.9)	13.6 (+4.7, ±0.9)
SSP5-8.5	3.7 (+6.6, ±1.6)	4.4 (+9.5, ±2.2)	2.1 (+10.4, ±2.4)	14.6 (+5.7, ±1.3)

Figure Captions

Fig. 1 – Distributions of the suitable climate space for permafrost peatlands in Europe and Western Siberia during the modern baseline period (1961–1990). Maps showing: a) the predictive performance of our palsa/peat plateau model; b) the predictive performance of our polygon mires model; and c) the distribution of gridded peat soil organic carbon content (hg m^{-2}), based on recent soil maps[1,65] (see methods for details) and coloured according to the predicted presence and absence of suitable climatic conditions for permafrost peatlands. For gridded peat soil organic carbon mass (Mt), see Figure S2. Map outlines are from ref[66].

Fig. 2 – Future climate space for permafrost peatlands in Europe and Western Siberia. Projected distributions of the suitable climate envelopes for palsas/peat plateaus and polygon mires in Europe and Western Siberia during the modern baseline period (1961–1990), and during 2090–2099 under four SSP scenarios: SSP1-2.6 (strong climate change mitigation), SSP2-4.5 (moderate mitigation), SSP3-7.0 (no mitigation baseline) and SSP5-8.5 (no mitigation, worst-case). For earlier projections from 2020–2029 to 2080–2089 see Figures S4–S7. Map outlines are from ref[66].

Fig. 3 – Comparisons of the total peat carbon (Gt) that is within the suitable climate envelopes for peatland permafrost in Europe and Western Siberia under four CMIP6 emission scenarios. Decadal time series showing for SSP1-2.6, SSP2-4.5, SSP3-7.0 and SSP5-8.5 the total peat soil organic carbon stock in Europe and Western Siberia that is: a) within the suitable climate envelope for palsas/peat plateaus; and b) within the suitable climate envelope for polygon mires. Whiskers indicate the full range of values from the 12 CMIP6 models in our ensemble, lower hinges indicate the 25th percentiles, upper hinges indicate the 75th percentiles, and centre lines indicate median values. Dashed lines represent the total peat soil organic carbon stock that is within the respective suitable climate envelopes during the modern baseline period (1961–1990). For comparisons of the total peatland area (km^2) that is within the suitable climate envelopes for peatland permafrost, see Figure S3.

Reference List

1 Hugelius, G. *et al.* Large stocks of peatland carbon and nitrogen are vulnerable to permafrost thaw. *Proc Natl Acad Sci U S A* **117**, 20438-20446, doi:10.1073/pnas.1916387117 (2020).

2 Davy, R. & Outten, S. The Arctic Surface Climate in CMIP6: Status and Developments since CMIP5. *J. Clim.* **33**, 8047-8068, doi:10.1175/jcli-d-19-0990.1 (2020).

3 Voigt, C. *et al.* Ecosystem carbon response of an Arctic peatland to simulated permafrost thaw. *Global Change Biol.* **25**, 1746-1764 (2019).

4 Swindles, G. T. *et al.* The long-term fate of permafrost peatlands under rapid climate warming. *Sci Rep* **5**, 17951, doi:10.1038/srep17951 (2015).

5 Du, R. *et al.* The role of peat on permafrost thaw based on field observations. *CATENA* **208**, 105772 (2022).

6 Chaudhary, N. *et al.* Modelling past and future peatland carbon dynamics across the pan-Arctic. *Glob Chang Biol* **26**, 4119-4133, doi:10.1111/gcb.15099 (2020).

7 Müller, J. & Joos, F. Committed and projected future changes in global peatlands–continued transient model simulations since the Last Glacial Maximum. *Biogeosciences* **18**, 3657-3687 (2021).

8 Seppälä, M. Synthesis of studies of palsa formation underlining the importance of local environmental and physical characteristics. *Quatern. Res.* **75**, 366-370 (2011).

9 Karjalainen, O. *et al.* High potential for loss of permafrost landforms in a changing climate. *Environmental Research Letters* **15**, doi:10.1088/1748-9326/abafd5 (2020).

10 Fan, X., Duan, Q., Shen, C., Wu, Y. & Xing, C. Global surface air temperatures in CMIP6: historical performance and future changes. *Environmental Research Letters* **15**, 104056 (2020).

11 Tebaldi, C. *et al.* Climate model projections from the scenario model intercomparison project (ScenarioMIP) of CMIP6. *Earth System Dynamics* **12**, 253-293 (2021).

12 Zoltai, S. & Tarnocai, C. Properties of a wooded palsa in northern Manitoba. *Arct. Alp. Res.* **3**, 115-129 (1971).

13 Minke, M., Donner, N., Karpov, N. S., de Klerk, P. & Joosten, H. Distribution, diversity, development and dynamics of polygon mires: examples from Northeast Yakutia (Siberia). *Peatlands International* **1**, 36-40 (2007).

14 O'Neill, H. B., Wolfe, S. A. & Duchesne, C. New ground ice maps for Canada using a paleogeographic modelling approach. *The Cryosphere* **13**, 753-773 (2019).

15 Fronzek, S., Luoto, M. & Carter, T. R. Potential effect of climate change on the distribution of palsa mires in subarctic Fennoscandia. *Clim. Res.* **32**, 1-12 (2006).

16 Luoto, M., Fronzek, S. & Zuidhoff, F. S. Spatial modelling of palsa mires in relation to climate in northern Europe. *Earth Surface Processes and Landforms: the Journal of the British Geomorphological Research Group* **29**, 1373-1387 (2004).

17 Peregon, A., Maksyutov, S., Kosykh, N. P. & Mironycheva-Tokareva, N. P. Map-based inventory of wetland biomass and net primary production in western Siberia. *Journal of Geophysical Research: Biogeosciences* **113** (2008).

18 Terentieva, I., Lapshina, E. D., Sabrekov, A. F., Maksyutov, S. S. & Glagolev, M. V. Mapping of West Siberian wetland complexes using landsat imagery: implications for methane emissions. (2017).

19 Zoltai, S., Siltanen, R. M. & Johnson, J. D. A wetland data base for the western boreal, subarctic, and arctic regions of Canada. 1-38 (Natural Resources Canada, Canadian Forest Service, Edmonton, Alberta, 2000).

20 Fewster, R. E. *et al.* Drivers of Holocene palsa distribution in North America. *Quaternary Science Reviews* **240**, doi:10.1016/j.quascirev.2020.106337 (2020).

21 Parviainen, M. & Luoto, M. Climate envelopes of mire complex types in Fennoscandia. *Geografiska Annaler: Series A, Physical Geography* **89**, 137-151 (2007).

22 Aalto, J., Harrison, S. & Luoto, M. Statistical modelling predicts almost complete loss of major periglacial processes in Northern Europe by 2100. *Nature communications* **8**, 1-8 (2017).

23 Eyring, V. *et al.* Overview of the Coupled Model Intercomparison Project Phase 6 (CMIP6) experimental design and organization. *Geoscientific Model Development* **9**, 1937-1958 (2016).

24 Brunner, L. *et al.* Reduced global warming from CMIP6 projections when weighting models by performance and independence. *Earth System Dynamics* **11**, 995-1012, doi:10.5194/esd-2020-23 (2020).

25 O'Neill, B. C. *et al.* The Scenario Model Intercomparison Project (ScenarioMIP) for CMIP6. *Geoscientific Model Development* **9**, 3461-3482, doi:10.5194/gmd-9-3461-2016 (2016).

26 Aalto, J., Venäläinen, A., Heikkinen, R. K. & Luoto, M. Potential for extreme loss in high-latitude Earth surface processes due to climate change. *Geophys. Res. Lett.* **41**, 3914-3924 (2014).

27 Halsey, L. A., Vitt, D. H. & Zoltai, S. C. Disequilibrium response of permafrost in boreal continental western Canada to climate change. *Clim. Change* **30**, 57-73 (1995).

28 Camill, P. & Clark, J. S. Climate change disequilibrium of boreal permafrost peatlands caused by local processes. *The American Naturalist* **151**, 207-222 (1998).

29 Borge, A. F., Westermann, S., Solheim, I. & Etzelmüller, B. Strong degradation of palsas and peat plateaus in northern Norway during the last 60 years. *The Cryosphere* **11**, 1-16 (2017).

30 Åkerman, H. J. & Johansson, M. Thawing permafrost and thicker active layers in sub-arctic Sweden. *Permafrost and periglacial processes* **19**, 279-292 (2008).

31 Olvmo, M., Holmer, B., Thorsson, S., Reese, H. & Lindberg, F. Sub-arctic palsa degradation and the role of climatic drivers in the largest coherent palsa mire complex in Sweden (Vissátvuopmi), 1955–2016. *Scientific reports* **10**, 1-10 (2020).

32 Payette, S., Delwaide, A., Caccianiga, M. & Beauchemin, M. Accelerated thawing of subarctic peatland permafrost over the last 50 years. *Geophys. Res. Lett.* **31** (2004).

33 Treat, C. C. *et al.* Effects of permafrost aggradation on peat properties as determined from a pan-Arctic synthesis of plant macrofossils. *Journal of Geophysical Research: Biogeosciences* **121**, 78-94 (2016).

34 Dearborn, K. D., Wallace, C. A., Patankar, R. & Baltzer, J. L. Permafrost thaw in boreal peatlands is rapidly altering forest community composition. *J. Ecol.* **109**, 1452-1467 (2021).

35 Olefeldt, D. & Roulet, N. T. Effects of permafrost and hydrology on the composition and transport of dissolved organic carbon in a subarctic peatland complex. *Journal of Geophysical Research: Biogeosciences* **117** (2012).

36 Burd, K., Estop-Aragonés, C., Tank, S. E. & Olefeldt, D. Lability of dissolved organic carbon from boreal peatlands: interactions between permafrost thaw, wildfire, and season. *Can. J. Soil Sci.* **100**, 503-515 (2020).

37 Klaminder, J., Yoo, K., Rydberg, J. & Giesler, R. An explorative study of mercury export from a thawing palsa mire. *Journal of Geophysical Research: Biogeosciences* **113** (2008).

38 Luoto, M. & Seppälä, M. Thermokarst ponds as indicators of the former distribution of palsas in Finnish Lapland. *Permafrost and Periglacial Processes* **14**, 19-27, doi:10.1002/ppp.441 (2003).

39 Vitt, D. H., Halsey, L. A. & Zoltai, S. C. The changing landscape of Canada's western boreal forest: the current dynamics of permafrost. *Canadian Journal of Forest Research* **30**, 283-287 (2000).

40 Turetsky, M., Wieder, R., Vitt, D., Evans, R. & Scott, K. The disappearance of relict permafrost in boreal north America: Effects on peatland carbon storage and fluxes. *Global Change Biol.* **13**, 1922-1934 (2007).

41 Jorgenson, M. T. *et al.* Resilience and vulnerability of permafrost to climate change. *Canadian Journal of Forest Research* **40**, 1219-1236 (2010).

42 Magnússon, R. Í. *et al.* Rapid vegetation succession and coupled permafrost dynamics in Arctic thaw ponds in the Siberian lowland tundra. *Journal of Geophysical Research: Biogeosciences* **125**, e2019JG005618 (2020).

43 Zoltai, S. Permafrost distribution in peatlands of west-central Canada during the Holocene warm period 6000 years BP. *Géographie physique et Quaternaire* **49**, 45-54 (1995).

44 Seppälä, M. in *Proceedings Fourth Canadian Permafrost Conference, Calgary. National Research Council of Canada, Ottawa.* 36-42.

45 Yu, Z., Loisel, J., Brosseau, D. P., Beilman, D. W. & Hunt, S. J. Global peatland dynamics since the Last Glacial Maximum. *Geophys. Res. Lett.* **37** (2010).

46 Harris, I., Osborn, T. J., Jones, P. & Lister, D. Version 4 of the CRU TS monthly high-resolution gridded multivariate climate dataset. *Scientific data* **7**, 1-18 (2020).

47 Serreze, M. C. & Barry, R. G. Processes and impacts of Arctic amplification: A research synthesis. *Global Planet. Change* **77**, 85-96 (2011).

48 Thurner, M. *et al.* Carbon stock and density of northern boreal and temperate forests. *Global Ecol. Biogeogr.* **23**, 297-310 (2014).

49 Seppälä, M. The origin of palsas. *Geografiska Annaler: Series A, Physical Geography* **68**, 141-147 (1986).

50 Mamet, S. D., Chun, K. P., Kershaw, G. G., Loranty, M. M. & Peter Kershaw, G. Recent increases in permafrost thaw rates and areal loss of palsas in the Western Northwest Territories, Canada. *Permafrost and periglacial processes* **28**, 619-633 (2017).

51 Camill, P. Permafrost thaw accelerates in boreal peatlands during late-20th century climate warming. *Clim. Change* **68**, 135-152 (2005).

52 Quinton, W. L. & Baltzer, J. The active-layer hydrology of a peat plateau with thawing permafrost (Scotty Creek, Canada). *Hydrogeology Journal* **21**, 201-220 (2013).

53 Turetsky, M. R., Wieder, R. K. & Vitt, D. H. Boreal peatland C fluxes under varying permafrost regimes. *Soil Biol. Biochem.* **34**, 907-912 (2002).

54 Schädel, C. *et al.* Potential carbon emissions dominated by carbon dioxide from thawed permafrost soils. *Nature climate change* **6**, 950-953 (2016).

55 Myers-Smith, I. H. & Hik, D. S. Climate warming as a driver of tundra shrubline advance. *J. Ecol.* **106**, 547-560 (2018).

56 Gibson, C. M. *et al.* Wildfire as a major driver of recent permafrost thaw in boreal peatlands. *Nature communications* **9**, 1-9 (2018).

57 Gibson, C. M., Estop-Aragonés, C., Flannigan, M., Thompson, D. K. & Olefeldt, D. Increased deep soil respiration detected despite reduced overall respiration in permafrost peat plateaus following wildfire. *Environmental Research Letters* **14**, 125001 (2019).

58 Estop-Aragonés, C. *et al.* Respiration of aged soil carbon during fall in permafrost peatlands enhanced by active layer deepening following wildfire but limited following thermokarst. *Environmental Research Letters* **13**, 085002 (2018).

59 Treat, C. C. *et al.* Predicted vulnerability of carbon in permafrost peatlands with future climate change and permafrost thaw in Western Canada. *Journal of Geophysical Research: Biogeosciences* **126**, e2020JG005872 (2021).

60 Jones, M. C. *et al.* Rapid carbon loss and slow recovery following permafrost thaw in boreal peatlands. *Global Change Biol.* **23**, 1109-1127 (2017).

61 Turetsky, M. R. *et al.* Carbon release through abrupt permafrost thaw. *Nature Geoscience* **13**, 138-143 (2020).

62 Heffernan, L., Estop-Aragonés, C., Knorr, K. H., Talbot, J. & Olefeldt, D. Long-term impacts of permafrost thaw on carbon storage in peatlands: deep losses offset by surficial accumulation. *Journal of Geophysical Research: Biogeosciences* **125**, e2019JG005501 (2020).

63 Gallego-Sala, A. V. *et al.* Latitudinal limits to the predicted increase of the peatland carbon sink with warming. *Nature Climate Change* **8**, 907-913 (2018).

64 Qiu, C. *et al.* The role of northern peatlands in the global carbon cycle for the 21st century. *Global Ecol. Biogeogr.* **29**, 956-973, doi:10.1111/geb.13081 (2020).

65 Hugelius, G. *et al.* Maps of northern peatland extent, depth, carbon storage and nitrogen storage. Dataset version 1.0. *Bolin Centre Database*. doi.org/10.17043/hugelius-2020 (2020).

66 Brownrigg, R. *mapdata: Extra Map Databases* https://CRAN.R-project.org/package=mapdata (2018).

Methods

Catalogue of Permafrost Peatland landforms

We collated all recorded locations of palsas/peat plateaus and polygon mires across the northern hemisphere using a structured literature search (Supplementary dataset S1). We searched for the terms “palsa”, “peat plateau”, “polygon mire”, “high-centre polygon”, “low-centre polygon”, and “permafrost peatland” alongside the names of selected regions (e.g. “Fennoscandia), countries (e.g. “Canada”), states (e.g. “Alaska”), Russian federal subjects (e.g. “Yamalo-Nenets Autonomous Okrug”), provinces and territories (e.g. “Quebec”) in Google Scholar. Other permafrost peatland types, such as permafrost fens[67], have been less readily observed and were not considered here. We prioritised research literature for which permafrost peatlands were the primary focus, but also scrutinised broader research publications that provided sufficient evidence to determine the type and location of individual landforms. Terminologies vary between regions, so where possible we used site descriptions and photographs to verify permafrost peatland classifications. The terms “palsa” and “peat plateau” are used interchangeably by some authors, so we combined these landforms into a single category. The focus of our study is permafrost peatlands. We did not consider permafrost landforms in non-peat soils (for example lithalsas, mineral palsas, or ice-wedge polygons in mineral soils) because such landforms are likely to respond differently to modern climate[68,69].

The original coordinates of each site were converted to a 0.5° × 0.5° spatial resolution, to match the spatial grid of the modern baseline climate data (see below) (Supplementary dataset S2). Sources varied in spatial resolution from site-specific studies to gridded 0.5° supervised classifications. Where landforms were reported without exact coordinates, we used site maps to record their location as the nearest 0.5° grid cell. Distributions of permafrost peatland landforms appear to be more fully defined in Fennoscandia, Western Siberia, and northern Alaska due to the availability of broad-scale gridded datasets[16-18,70], which were lacking for Canada, and eastern and central Siberia. Polygon mire presence in northern Alaska was principally identified using a remotely-sensed classification of polygonal tundra[70], with the presence of peat verified by local surface lithology descriptions[71]. Our final catalogue presents a binary map for the presence of palsas/peat plateaus and polygon mires across the

northern hemisphere. Our catalogue expands on the North American catalogue of palsas/peat plateaus by ref[20], with 1,199 additional sites from Europe and Siberia, and 553 observations of polygon mires from across the pan-Arctic (2,102 total sites) (see Figure S1 and supplementary dataset S1). We set the southern limit of our study domain to be 44°N to encompass all observed permafrost peatland landforms.

Modern Distribution of Northern Peatlands

To estimate the modern distribution of northern peatlands, we primarily used the PEATMAP database[72]. PEATMAP shapefiles were rasterised, reclassified, and sampled in ArcGIS to produce a binary map of peatland presence/absence for each 0.5° × 0.5° grid cell north of 44°N. We improved our estimate of modern peat coverage in northern Alaska using the peat distribution map constructed by ref[20], and reclassified a small portion of grid cells that were classified as non-peat containing by these peatland maps, but which contained observations of palsas/peat plateaus or polygon mires.

Study Domain

Our study domain consists of European and Western Siberian peatlands, which we define as all terrestrial 0.5° × 0.5° grid cells that contain evidence of peat, and which are located north of 44°N and between 25°W and 95°E (4,615 grid cells in total). We focused our analyses on Europe and Western Siberia because the spatial extents of palsa, peat plateaus and polygon mires are much better constrained here than in other northern areas. Our study domain omits most of central Siberia, and all of eastern Siberia. Our literature search returned only 10 observations of permafrost peat landforms east of 95°E, which we believe severely underestimates their true extent. Although the number of records in Canada and Alaska was higher (367 grid cells contained permafrost peatland observations), the density of these observations was low compared to Europe and Western Siberia (where 934 grid cells contained permafrost peatland observations) and their distribution was patchy (Figure S1). Previous broad-scale mapping products indicate that several parts of Canada that lack observations are extensively covered by peatlands[72] and permafrost[73], suggesting that the

locations of some permafrost peatland landforms in North America are missing from published records[20]. For this reason, our study domain also omits North America. We only considered grid cells in Europe and Western Siberia that presently contain peat, because any new peat deposits that form outside of this domain are unlikely to reach a sufficient thickness to support permafrost peatland landforms before 2100. The remaining 4,615 grid cells in our study domain therefore represent plausible locations for permafrost peatland landforms to exist during the 21st century.

Estimation of Northern Peatland SOC stocks

We analysed the soil organic carbon (SOC) maps of histels and histosols by ref[1] in QGIS to produce gridded estimates of peatland soil carbon (available from: https://bolin.su.se/data/hugelius-2020). These maps combined core-based analyses with machine-learning methods and showed greater spatial coverage than previous products[74]. The maps estimate that histosols north of 23°N contain 230 ± 81 Gt SOC, whilst histels contain 185 ± 66 Gt SOC (see ref[1] for details on agreement with previous estimates). These SOC stocks have high associated uncertainties caused by high spatial variation in peat depths and sampling densities, but represent the best gridded estimates of northern peat carbon currently available. Although histel and histosol maps include peatlands, they may also include other organic soils, such as mucks that are more heavily decomposed than peat[75]. To improve confidence in our estimates, we therefore used our mapped extent of northern peatlands (described above) to only calculate SOC values for grid cells that are known to contain peat. This does necessarily assume that for grid cells where peat is present, the carbon mass of histosols and histels refers solely to peat soils, which may lead to some overestimation where non-peat organic soils are also present.

To estimate the peat soil organic carbon mass (SOCM) (hg) of each 0.5° grid cell, we first converted the soil organic carbon content (SOCC) (hg m^{-2}) maps by ref[1] from rasters to polygons, and intersected any polygons that extended across more than one grid cell. We calculated the surface area of each SOCC polygon and grid cell using the data's original World Azimuthal Equidistant projection. We then multiplied the surface area of each polygon by its SOCC and aggregated these values to the 0.5° grid cell in which they were located. To provide

SOCC estimates at 0.5° spatial resolution, we divided our gridded estimates for SOCM by the surface area of each 0.5° grid cell. SOC data were available for all 4,615 peat containing grid cells in our study area for Europe and Western Siberia, equating to a total SOC stock of 141.1 Gt.

Modern climate data

We used a custom Python script (available from https://github.com/refewster/Imminent-loss-of-climate-space-for-Eurasian-permafrost-peatlands-) to extract and average mean monthly temperature and precipitation values during 1961–1990 from the gridded CRU TS 4.04 climatology[46] to represent modern baseline climate. We selected the period 1961–1990 to reduce any disequilibrium[27] between landform distributions and the modern climate data, because the magnitude of anthropogenic climate change was less than at present[20]. The use of an earlier time period was deemed unsuitable because climate station coverage at high latitudes increased substantially during the second half of the 20th century, particularly in Eastern Europe and the Arctic where several regions previously lacked observational precipitation data[46]. Furthermore, previous climate envelope modelling of North American palsas/peat plateaus found models fitted to climate data from 1961–1990 performed better than equivalent models fitted to general circulation model (GCM) simulations of preindustrial climate[20]. We obtained modern baseline climate data for all 4,615 grid cells within our study domain.

Future climate simulations

We obtained projected decadal 21st century climate projections from an ensemble of 12 GCMs included in the Coupled Model Intercomparison Project 6 (CMIP6)[23], to represent future climates. To build our ensemble, we selected one CMIP6 GCM from each of the model groupings by ref[24] to ensure that our GCMs were independent from one another (i.e. without shared components or a common origin). Where multiple candidate GCMs were available, we selected the model from each grouping which displayed the highest native spatial resolution, and which simulated historical climates for our study region that most closely reproduced the

mean temperature and precipitation values from our modern observational climatology for the period 1961-1990 (see above). Some CMIP6 models have a very high equilibrium climate sensitivity (ECS) of > 5°C, but none of these models were chosen by our model selection criteria and they were therefore not included in this study. Some studies have shown that CMIP6 model ensembles project lower warming when constrained by historical observational trends[76] or model weighting metrics[24], but such constraints were not applied to our simulations. We obtained our CMIP6 climate projections from the Earth System Grid Federation (https://esgf-node.llnl.gov/search/cmip6/). Our final ensemble has an equilibrium climate sensitivity range of 1.9–4.8°C (median of 3.0°C) (Table S1), which closely aligns with the IPCC Assessment Report 6 "very likely" range of 2.0–5.0°C (best estimate = 3.0°C)[77]. Our ensemble presents greater warming than CMIP5 ensembles, but slightly less warming than if all CMIP6 models were included[78].

We used a custom Python script (available from https://github.com/refewster/Imminent-loss-of-climate-space-for-Eurasian-permafrost-peatlands-) to extract and average projected mean monthly temperature and precipitation values for each decade during 2020–2099. We first converted temperature values from Kelvin (K) to degrees Celsius (°C) and converted precipitation values from mean precipitation flux (kg m^{-2} s^{-1}) to mean monthly totals (mm). We then downscaled and bias-corrected CMIP6 outputs to a 0.5° × 0.5° spatial resolution, following an almost identical method to ref[79]. This downscaling procedure retains terrestrial climates for islands and coastlines by initially extrapolating terrestrial climate data across the domain using a Poisson equation solver with overrelaxation. To downscale our climate data to a 0.5° × 0.5° spatial resolution, we favoured the use of bilinear interpolation over the bicubic spline approach used by ref[79], because this approach is more widely used in climate science, and because bicubic interpolation can cause unrealistically high climatic variability[80]. We then used the CRU TS 4.04 land-sea mask to remove all oceanic 0.5° grid cells, resulting in an output that matched the spatial domain of the modern baseline climate data. We corrected for spatial biases in our downscaled CMIP6 future climate projections, again using the method of ref[79]. For temperature, we calculated the anomaly in simulated temperatures between the historical (1961–1990) and future time periods (from 2020–2029 to 2090–2099), and added this anomaly to the relevant observational mean (covering 1961–1990). For precipitation, we multiplied our simulated future precipitation values by a correction factor,

derived from simulated and observational precipitation values for the historical baseline period (1961–1990) (see ref[79] for full details).

Statistical Modelling and Evaluation

We fitted two climate envelope models to statistically predict the modern baseline (1961–1990) and future distributions of palsas/peat plateaus and polygon mires in Europe and Western Siberia (see above for study domain details). We used one-vs-all (OVA) binary logistic regression to fit our climate envelope models, where the two landform classes (palsas/peat plateaus, and polygon mires) were considered as a separate binary response[81]. Logistic regression models relate binary observations to continuous predictors and have previously predicted palsa/peat plateau distributions in North America[20] and Fennoscandia[16]. Multinomial logistic regression was unsuitable for this purpose because this method requires mutually exclusive classes[82] and our study domain included 76 grid cells where both palsas/peat plateaus and polygon mires were present. We then drove our climate envelope models with projections of future climate from 12 CMIP6 models (Table S1) and calculated the median agreement of predicted presence/absence.

To fit our bioclimatic models, we selected five candidate climate variables that have previously been linked to permafrost peatland distributions in Fennoscandia[15,16,21,22,83,84] and North America[20]: mean annual temperature (*MAT)*; annual temperature range *(TRANGE)*; growing degree days (GDD_5); rain precipitation (*RAINFALL*); and snow precipitation (*SNOWFALL*) (see Table S10 for variable descriptions). We calculated each climate variable from mean monthly temperature and precipitation values, following ref[20]. We did not constrain our modelling with other non-climatic factors, such as the composition of peatland vegetation or peat cover thickness, because suitable geospatial data were unavailable. Multicollinearity was evident in our modern baseline climate dataset, with all five climatic predictor variables found to be significantly correlated with one another ($p < 0.025$) according to a Spearman's Rank correlation matrix (Table S11). Multicollinearity of climatic predictors was present in grid cells with and without landform observations (Tables S12 and S13). Whilst climate variables are often highly correlated, the presence of multicollinearity means that individual predictor coefficients in our models should be interpreted with caution, even if the

model predictions as a whole can be considered robust[85]. Additionally, strong correlations between predictors can, in some cases, cause significant predictors to be incorrectly excluded during model calibration and can impact model performance where predictions are extrapolated to a different time or place[85,86]. To limit multicollinearity, we omitted several similar variables from our modelling at an early stage. The frost number (*FROST*) has previously been linked to permafrost distributions at broad spatial scales[87], but was too closely correlated with *MAT* for both variables to be included reliably. We experimented with preliminary models fitted with each variable separately and found that those models that included *MAT* consistently outperformed those fitted with *FROST*. Furthermore, we included seasonal rather than annual precipitation metrics so that the insulating properties of snow cover[22] and dry soils[8] could be represented individually in our modelling. Cross-validated evaluation statistics, generated by splitting the data randomly into separate calibration and evaluation subsets, are almost identical to those from models fitted to the full domain (Table S4), giving us confidence in the predictive capabilities of our final models (see below for full details).

We fitted our logistic regression models (Tables S2 and S3) in IBM SPSS Statistics 23 following the method of ref[20]. We entered all five climatic predictors simultaneously (block entry), alongside the squared form of each variable (*MAT**, $TRANGE^2$, $RAINFALL^2$, $SNOWFALL^2$ and $GDD_5{}^2$). We calculated *MAT** as the product of *MAT* and its absolute value, |*MAT*|, to retain the sign of negative temperatures in its quadratic term. We sequentially removed non-significant pairs of predictors (e.g. *TRANGE* and $TRANGE^2$) using a stepwise backwards-deletion approach, until all remaining untransformed predictors significantly contributed to the model's predictive performance (based on deviance scores). Where untransformed predictor variables were found to be significant predictors of landform presence, we retained their quadratic terms irrespective of their significance, because previous studies have shown that permafrost peatland landforms exist within optimum climatic windows and do not relate linearly to climate[16,20]. We used Bonferroni correction to select a stricter significance criterion for predictor removal (Student's t; $p < 0.025$ threshold) than ref[20], to limit the occurrence of Type I errors (i.e. non-significant variables falsely appearing to be significant) when fitting two models to the same training set[88]. We then tested the addition of several first-order interaction terms (i.e. two variables multiplied together to form a single, combined predictor).

To prevent spurious predictions where future climates exceeded modern climatic ranges, we added a plausibility criterion to nullify model predictions in grid cells where *RAINFALL* exceeded 1,500 mm yr^{-1}, which is more than twice the maximum rainfall (729 mm yr^{-1}) under which palsas/peat plateaus or polygon mires presently exist[20]. We calculated standardised parameter coefficients (β_s) for each predictor variable following ref[89].

To make predictions with a logistic regression model, the continuous response variable (predicted probability) is classified into a binary prediction of presence/absence according to a threshold probability, which we refer to as the classification threshold. Positive cases (observations of landform presence) in our training set for Europe and Western Siberia were relatively rare (only 934 or 20 % of the 4,615 grid cells contained permafrost peatland landforms). We therefore selected an optimised classification threshold for each of our models that maximised model informedness (see below), a metric that is unaffected by case prevalence[20,90]. Our final climate envelope model for palsas/peat plateaus has an optimised classification threshold of 0.273, and our model for polygon mires has an optimised classification threshold of 0.130 (outputs shown in Figures 1 and 2).

We evaluated the predictive classifications of our logistic regression models using three complementary evaluation metrics: accuracy, informedness, and the area under the curve (AUC) of a receiver operating characteristic plot[20,90] (Table S4). Accuracy evaluates the proportion (0–1) of correctly classified cases (both presence and absence)[90]. Informedness evaluates both presence and absence to assess how informed a model's prediction is compared to chance, and how consistently a model can correctly predict a case, with values ranging from 1 (all cases classified correctly) through 0 (random predictions) to -1 (all cases classified incorrectly)[90]. AUC is also unaffected by case prevalence but compares predictions across all possible classification thresholds, with scores ranging from 0.5 (random classification) to 1 (perfect classification)[91].

To assess the predictive performance of our climate envelope modelling for predicting data points outside of the model calibration setting, we used five-fold cross-validation. We split our modern climate dataset into five random subsets of similar size. For palsas/peat plateaus and polygon mires in turn, we used four subsets to calibrate a model, which we then used to predict landform presence/absence in a fifth, unused validation subset. From this prediction,

we calculated model accuracy, informedness, and AUC. We repeated this process five times for palsas/peat plateaus and polygon mires respectively, each time omitting a different subset from the calibration set to be used for model evaluation. We then used these validation set predictions to calculate the cross-validated mean and standard error of each performance metric for each model type (palsas/peat plateaus and polygon mires) (Table S4). Final parameter estimates for both climate envelope models were calibrated from the full modern climate dataset, and not from cross-validation subsets.

Data availability

The modern observational climate data was extracted from the CRU TS 4.04 dataset (https://crudata.uea.ac.uk/cru/data/hrg/cru_ts_4.04/), the CMIP6 projections of 21st century climate are available at their native resolution from the Earth System Grid Federation (https://esgf-node.llnl.gov/search/cmip6/), the modern peatland extents were primarily estimated using PEATMAP (http://archive.researchdata.leeds.ac.uk/251/), and the original soil organic carbon maps are available from the Bolin Centre Database (https://bolin.su.se/data/hugelius-2020). Any remaining data used to produce this research are included in the supplementary information, and in supplementary datasets S1 and S2.

Code availability

The Python code used to extract modern climate normals, and to downscale and bias-correct CMIP6 climate projections is available from: https://github.com/refewster/Imminent-loss-of-climate-space-for-Eurasian-permafrost-peatlands-.

Methods Reference List

67 Olefeldt, D., Turetsky, M. R., Crill, P. M. & McGuire, A. D. Environmental and physical controls on northern terrestrial methane emissions across permafrost zones. *Global Change Biol.* **19**, 589-603 (2013).

68 Pissart, A. Palsas, lithalsas and remnants of these periglacial mounds. A progress report. *Progress in Physical Geography* **26**, 605-621 (2002).

69 Wolfe, S. A., Stevens, C. W., Gaanderse, A. J. & Oldenborger, G. A. Lithalsa distribution, morphology and landscape associations in the Great Slave Lowland, Northwest Territories, Canada. *Geomorphology* **204**, 302-313 (2014).

70 Lara, M. J., Nitze, I., Grosse, G. & McGuire, A. D. Tundra landform and vegetation productivity trend maps for the Arctic Coastal Plain of northern Alaska. *Scientific data* **5**, 180058 (2018).

71 Jorgenson, M. T. & Grunblatt, J. Landscape-level ecological mapping of northern alaska and field site photography., (Arctic Landscape Conservation Cooperative, U.S. Fish & Wildlife Service, Fairbanks, Alaska, 2013).

72 Xu, J., Morris, P. J., Liu, J. & Holden, J. PEATMAP: Refining estimates of global peatland distribution based on a meta-analysis. *Catena* **160**, 134-140 (2018).

73 Brown, J., Ferrians Jr, O., Heginbottom, J. A. & Melnikov, E. *Circum-Arctic map of permafrost and ground-ice conditions*. (US Geological Survey Reston, VA, 1997).

74 Hugelius, G. *et al.* The Northern Circumpolar Soil Carbon Database: spatially distributed datasets of soil coverage and soil carbon storage in the northern permafrost regions. *Earth System Science Data* **5**, 3 (2013).

75 Everett, K. R. in *Developments in Soil Science* Vol. 11 1-53 (Elsevier, 1983).

76 Tokarska, K. B. *et al.* Past warming trend constrains future warming in CMIP6 models. *Science Advances* **6**, eaaz9549 (2020).

77 Forster, P. *et al.* in *Climate Change 2021: The Physical Science Basis. Contribution of Working Group I to the Sixth Assessment Report of the Intergovernmental Panel on Climate Change* Ch. Chapter 7: The Earth's Energy Budget, Climate Feedbacks, and Climate Sensitivity, (Cambridge University Press, 2021).

78 Flynn, C. M. & Mauritsen, T. On the climate sensitivity and historical warming evolution in recent coupled model ensembles. *Atmospheric Chemistry and Physics* **20**, 7829-7842 (2020).

79 Morris, P. J. *et al.* Global peatland initiation driven by regionally asynchronous warming. *Proceedings of the National Academy of Sciences* **115**, 4851-4856 (2018).

80 Latombe, G. *et al.* Comparison of spatial downscaling methods of general circulation model results to study climate variability during the Last Glacial Maximum. *Geoscientific Model Development* **11**, 2563-2579 (2018).

81 Galar, M., Fernández, A., Barrenechea, E., Bustince, H. & Herrera, F. An overview of ensemble methods for binary classifiers in multi-class problems: Experimental study on one-vs-one and one-vs-all schemes. *Pattern Recognition* **44**, 1761-1776 (2011).

82 Petrucci, C. J. A primer for social worker researchers on how to conduct a multinomial logistic regression. *Journal of social service research* **35**, 193-205 (2009).

83 Fronzek, S. *et al.* Evaluating sources of uncertainty in modelling the impact of probabilistic climate change on sub-arctic palsa mires. *Natural Hazards & Earth System Sciences* **11** (2011).

84 Aalto, J. & Luoto, M. Integrating climate and local factors for geomorphological distribution models. *Earth Surface Processes and Landforms* **39**, 1729-1740 (2014).

85 Graham, M. H. Confronting multicollinearity in ecological multiple regression. *Ecology* **84**, 2809-2815 (2003).

86 Dormann, C. F. *et al*. Collinearity: a review of methods to deal with it and a simulation study evaluating their performance. *Ecography* **36**, 027–046 (2013).

87 Anisimov, O. A. & Nelson, F. E. Permafrost zonation and climate change in the northern hemisphere: results from transient general circulation models. *Clim. Change* **35**, 241-258 (1997).

88 Armstrong, R. A. When to use the B onferroni correction. *Ophthalmic and Physiological Optics* **34**, 502-508 (2014).

89 Menard, S. Standards for Standardized Logistic Regression Coefficients. *Social Forces* **89**, 1409-1428 (2011).

90 Powers, D. M. Evaluation: from precision, recall and F-measure to ROC, informedness, markedness and correlation.(2011). (2011).

91 Pearce, J. & Ferrier, S. Evaluating the predictive performance of habitat models developed using logistic regression. *Ecol. Model.* **133**, 225-245 (2000).

Supplemental information

Table S1 – General circulation models included in our CMIP6 model ensemble. Outputs from these models were used to represent future climates. Transient climate response (TCR) (°C) and equilibrium climate sensitivity (ECS) (°C) scores are taken from ref[1].

Model	TCR (°C)	ECS (°C)
INM-CM5-0	-	1.9
CAMS-CSM1-0	1.7	2.3
MIROC6	1.6	2.6
GFDL-ESM4	1.6	2.6
MPI-ESM1-2-HR	1.7	3.0
FGOALS-f3-L	2.1	3.0
BCC-CSM2-MR	1.7	3.0
MRI-ESM2-0	1.6	3.2
IPSL-CM6A-LR	2.3	4.6
ACCESS-CM2	2.1	4.7
CESM2-WACCM	2.0	4.8
CNRM-CM6-1	2.1	4.8

Table S2 – Summary of the logistic regression model which describes the modern climate envelope of palsas/peat plateaus in Europe and Western Siberia. *βs* are standardised coefficients, according to the method of ref[2].

Variable	Coefficient	Standard error	*βs*	*t*	Significance
Constant	7.091×10^{1}	8.719	-	8.133	< 0.001
MAT	-4.616	3.369×10^{-1}	-9.708×10^{-1}	-13.703	< 0.001
*MAT**	3.030×10^{-1}	2.286×10^{-2}	5.251×10^{-1}	13.254	< 0.001
TRANGE	-4.371	3.863×10^{-1}	-1.493	-11.314	< 0.001
$TRANGE^2$	4.221×10^{-2}	3.941×10^{-3}	7.948×10^{-1}	10.709	< 0.001
GDD_5	2.232×10^{-2}	2.871×10^{-3}	6.646×10^{-1}	7.776	< 0.001
GDD_5^2	-7.653×10^{-6}	1.013×10^{-6}	-9.621×10^{-1}	-7.556	< 0.001
RAINFALL	-1.169×10^{-1}	1.930×10^{-2}	-1.290	-6.054	< 0.001
$RAINFALL^2$	1.998×10^{-5}	4.760×10^{-6}	4.394×10^{-1}	4.198	< 0.001
SNOWFALL	-2.291×10^{-2}	4.850×10^{-3}	-9.405×10^{-2}	-4.723	< 0.001
$SNOWFALL^2$	1.925×10^{-5}	6.961×10^{-6}	4.777×10^{-2}	2.765	0.006
RAINFALL × *TRANGE*	3.804×10^{-3}	5.299×10^{-4}	4.266×10^{-1}	7.179	< 0.001

Table S3 – Summary of the logistic regression model which describes the modern climate envelope of polygon mires in Europe and Western Siberia. *βs* are standardised coefficients, according to the method of ref[2].

Variable	Coefficient	Standard error	*βs*	*t*	Significance
Constant	-3.066×10^{1}	3.372	-	-9.092	< 0.001
MAT	-6.739	5.384×10^{-1}	-9.316×10^{-1}	-12.517	< 0.001
*MAT**	3.865×10^{-1}	3.251×10^{-2}	4.404×10^{-1}	11.888	< 0.001
SNOWFALL	6.271×10^{-2}	2.122×10^{-2}	1.693×10^{-1}	2.955	0.003
$SNOWFALL^2$	-2.153×10^{-4}	4.905×10^{-5}	-3.512×10^{-1}	-4.388	< 0.001

Table S4 – Cross-validated model performance statistics and optimised classification thresholds for our climate envelope models of palsas/peat plateaus and polygon mires for Europe and Western Siberia (from 25°W to 95°E). Mean values (and standard errors) for each evaluation metric were calculated from predictions generated from five validation subsets. We optimised the classification thresholds for each model, because of the imbalance of landform presence and absence in our training datasets (see methods for further details).

Metric	Palsas/peat plateaus	Polygon Mires
Accuracy	94.1 % (± 0.004)	96.1 % (± 0.005)
Informedness	0.886 (± 0.006)	0.936 (± 0.003)
AUC	0.982 (± 0.002)	0.991 (± 0.002)
Optimised classification threshold	0.273	0.130

Table S5 – Predicted climate envelopes for palsas/peat plateaus and polygon mires in Europe and Western Siberia (from 25°W to 95°E), estimated using our logistic regression models (Tables S2–S3) for the modern baseline period (1961–1990). Spatial minima, medians and maxima are presented, calculated from climatically suitable grid cells. Hyphens represent non-significant climate variables.

Climate Envelope		*MAT* (°C)	*TRANGE* (°C)	GDD_5 (°C days)	*RAINFALL* (mm yr^{-1})	*SNOWFALL* (mm yr^{-1})
Palsas/peat plateaus	Min	-9.4	11.6	0	141	130
	Median	-4.7	38.2	1246	283	222
	Max	2.6	43.5	1672	471	751
Polygon Mires	Min	-12.1	-	-	-	108
	Median	-8.3	-	-	-	209
	Max	-5.2	-	-	-	297

Table S6 – Median projected values of regional annual temperature range (*TRANGE*) by 2090–2099; the change from the modern baseline period (1961–1990) (Δ *TRANGE*); and standard deviations of *TRANGE* across our CMIP6 model ensemble (Std. dev). *TRANGE* values were averaged across all grid cells that were classified to be climatically suitable for palsas/peat plateaus and polygon mires during the modern baseline period (Figure 2), for Fennoscandia and Russia. Our Russia region excludes the Kola Peninsula and Karelia, which are included in Fennoscandia.

Scenario	*TRANGE* (Δ *TRANGE*, Std. dev) (°C)		
	Palsas/peat plateaus in Fennoscandia	Palsas/peat plateaus in Russia	Polygon mires in Russia
SSP1-2.6	27.1 (-0.7, ±1.9)	37.9 (-0.6, ±1.7)	35.5 (-1.4, ±2.1)
SSP2-4.5	26.5 (-1.3, ±1.9)	37.3 (-1.2, ±1.5)	35.1 (-1.7, ±1.7)
SSP3-7.0	25.6 (-2.2, ±2.2)	36.1 (-2.3, ±2.4)	33.1 (-3.7, ±2.4)
SSP5-8.5	26.2 (-1.6, ±2.0)	35.0 (-3.5, ±3.0)	32.6 (-4.2, ±3.6)

Table S7 – Projected regional growing degree days (GDD_5) for 2090–2099, with comparisons to the modern baseline period (1961–1990). See Table S6 caption for full details.

Scenario	GDD_5 (Δ GDD_5, Std. dev) (°C days)		
	Palsas/peat plateaus in Fennoscandia	Palsas/peat plateaus in Russia	Polygon mires in Russia
SSP1-2.6	1419 (+496, ±208)	1615 (+322, ±160)	1249 (+428, ±168)
SSP2-4.5	1639 (+716, ±155)	1876 (+583, ±213)	1442 (+621, ±209)
SSP3-7.0	1892 (+968, ±227)	2167 (+874, ±307)	1648 (+827, ±241)
SSP5-8.5	1970 (+1046, ±349)	2591 (+1298, ±425)	2049 (+1227, ±391)

Table S8 – Projected regional rainfall for 2090–2099, with comparisons to the modern baseline period (1961–1990). See Table S6 caption for full details.

Scenario	*RAINFALL* (Δ *RAINFALL*, Std. dev) (mm yr^{-1})		
	Palsas/peat plateaus in Fennoscandia	Palsas/peat plateaus in Russia	Polygon mires in Russia
SSP1-2.6	357 (+69, ±27)	317 (+35, ±29)	230 (+33, ±20)
SSP2-4.5	407 (+118, ±29)	362 (+80, ±34)	250 (+53, ±37)
SSP3-7.0	445 (+156, ±39)	374 (+91, ±39)	308 (+111, ±48)
SSP5-8.5	472 (+183, ±58)	418 (+136, ±52)	328 (+131, ±58)

Table S9 – Projected regional snowfall for 2090–2099, with comparisons to the modern baseline period (1961–1990). See Table S6 caption for full details.

Scenario	*SNOWFALL* (Δ *SNOWFALL*, Std. dev) (mm yr^{-1})		
	Palsas/peat plateaus in Fennoscandia	Palsas/peat plateaus in Russia	Polygon mires in Russia
SSP1-2.6	243 (-29, ±25)	234 (+14, ±25)	224 (+15, ±21)
SSP2-4.5	243 (-30, ±17)	219 (-1, ±22)	233 (+24, ±21)
SSP3-7.0	233 (-40, ±22)	226 (+6, ±22)	225 (+16, ±26)
SSP5-8.5	233 (-39, ±27)	217 (-3, ±33)	215 (+6, ±34)

Table S10 – Description of candidate climate variables.

Variable	Description	Units
Mean annual temperature (*MAT*)	Average annual air temperature	°C
Temperature range (*TRANGE*)	Difference between maximum and minimum monthly air temperatures	°C
Growing degree days (GDD_5)	Annual time integral of monthly air temperatures above 5°C	°C days
Rain precipitation (*RAINFALL*)	Total annual precipitation in months with average air temperatures > 0°C	mm yr^{-1}
Snow precipitation (*SNOWFALL*)	Total annual precipitation in months with average air temperatures < 0°C	mm yr^{-1}

Table S11 – Spearman's Rank correlation matrix for candidate climate variables included in our climate envelope modelling of Europe and Western Siberia. Correlation coefficients, r_s, and significance values, p, are presented. See Table S10 for variable descriptions.

	MAT	*TRANGE*	*GDD5*	*RAINFALL*	*SNOWFALL*
MAT	-	$p < 0.001$	$p < 0.001$	$p < 0.001$	$p < 0.001$
TRANGE	$r_s = -0.783$	-	$p < 0.001$	$p < 0.001$	$p < 0.001$
GDD5	$r_s = 0.897$	$r_s = -0.473$	-	$p < 0.001$	$p < 0.001$
RAINFALL	$r_s = 0.877$	$r_s = -0.773$	$r_s = 0.732$	-	$p < 0.001$
SNOWFALL	$r_s = -0.627$	$r_s = 0.390$	$r_s = -0.707$	$r_s = -0.438$	-

Table S12 – Spearman's Rank correlation matrix for candidate climate variables for grid cells in Europe and Western Siberia where observations of palsas/peat plateaus are present (n = 671) and absent (n = 3,944). Correlation coefficients, r_s, and significance values, p, are presented. See Table S10 for variable descriptions.

		MAT	*TRANGE*	*GDD5*	*RAINFALL*	*SNOWFALL*
MAT	*Presence*		$p = 0.213$	$p < 0.001$	$p < 0.001$	$p = 0.036$
	Absence		$p < 0.001$	$p < 0.001$	$p < 0.001$	$p < 0.001$
TRANGE	*Presence*	$r_s = -0.048$		$p < 0.001$	$p < 0.001$	$p = 0.014$
	Absence	$r_s = -0.787$		$p < 0.001$	$p < 0.001$	$p < 0.001$
GDD5	*Presence*	$r_s = 0.390$	$r_s = 0.825$		$p < 0.001$	$p = 0.011$
	Absence	$r_s = 0.879$	$r_s = -0.455$		$p < 0.001$	$p < 0.001$
RAINFALL	*Presence*	$r_s = 0.712$	$r_s = 0.385$	$r_s = 0.668$		$p = 0.056$
	Absence	$r_s = 0.857$	$r_s = -0.816$	$r_s = 0.670$		$p < 0.001$
SNOWFALL	*Presence*	$r_s = -0.081$	$r_s = 0.095$	$r_s = -0.098$	$r_s = 0.074$	
	Absence	$r_s = -0.636$	$r_s = 0.359$	$r_s = -0.724$	$r_s = -0.413$	

Table S13 – Spearman's Rank correlation matrix for candidate climate variables for grid cells in Europe and Western Siberia where observations of polygon mires are present (n = 339) and absent (n = 4,276). Correlation coefficients, r_s, and significance values, p, are presented. See Table S10 for variable descriptions.

		MAT	*TRANGE*	*GDD5*	*RAINFALL*	*SNOWFALL*
MAT	*Presence*		$p < 0.001$	$p < 0.001$	$p < 0.001$	$p < 0.001$
	Absence		$p < 0.001$	$p < 0.001$	$p < 0.001$	$p < 0.001$
TRANGE	*Presence*	$r_s = 0.802$		$p < 0.001$	$p < 0.001$	$p = 0.001$
	Absence	$r_s = -0.810$		$p < 0.001$	$p < 0.001$	$p < 0.001$
GDD5	*Presence*	$r_s = 0.983$	$r_s = 0.864$		$p < 0.001$	$p < 0.001$
	Absence	$r_s = 0.874$	$r_s = -0.473$		$p < 0.001$	$p < 0.001$
RAINFALL	*Presence*	$r_s = 0.797$	$r_s = 0.555$	$r_s = 0.800$		$p < 0.001$
	Absence	$r_s = 0.854$	$r_s = -0.807$	$r_s = 0.676$		$p < 0.001$
SNOWFALL	*Presence*	$r_s = 0.401$	$r_s = 0.181$	$r_s = 0.408$	$r_s = 0.835$	
	Absence	$r_s = -0.696$	$r_s = 0.414$	$r_s = -0.786$	$r_s = -0.488$	

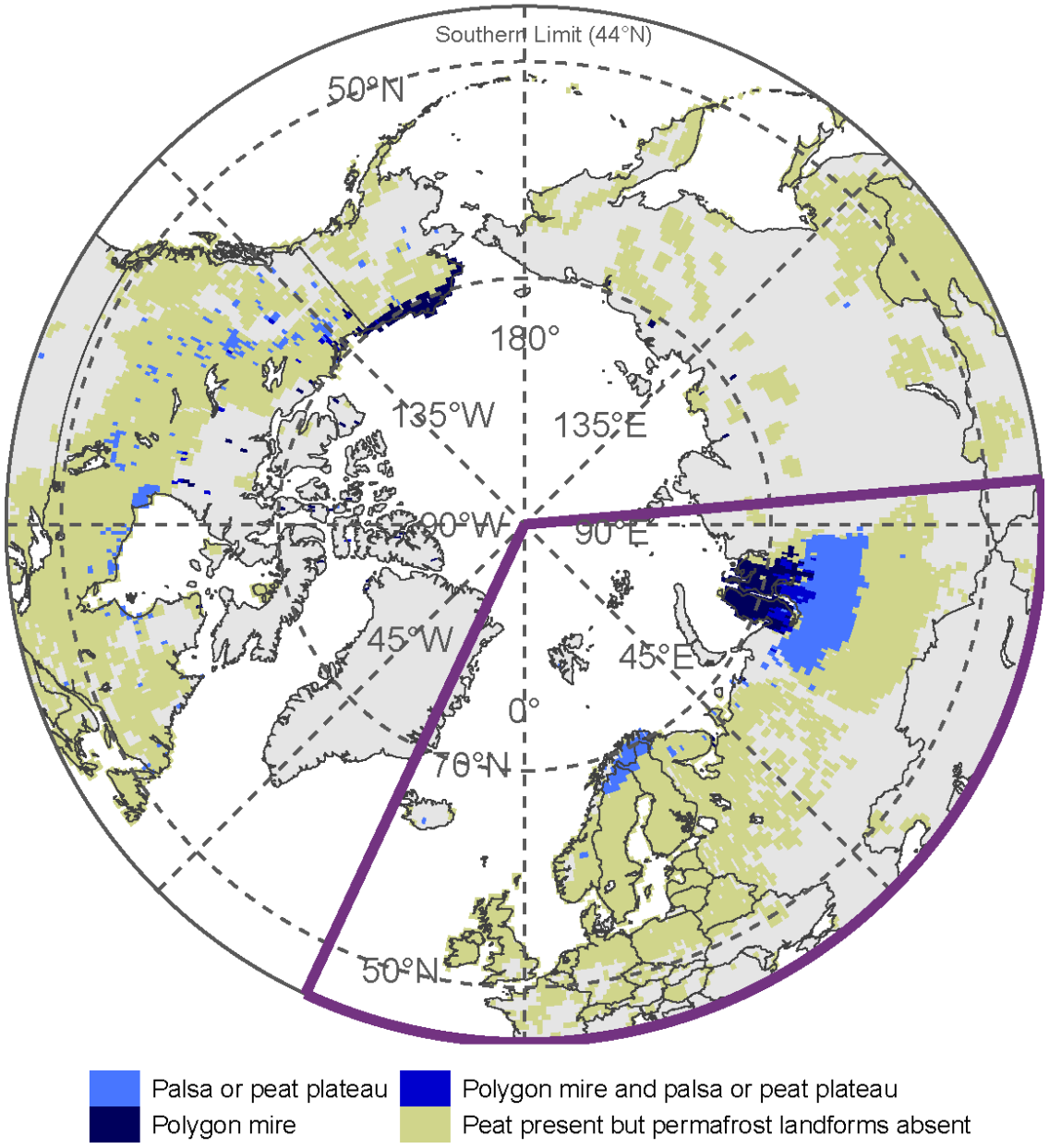

Figure S1 – Distribution of observed permafrost peatland landforms in our catalogue of published records (Dataset S1). Dark purple box indicates our study domain (north of 44°N and between 25°W and 95°E). Map outlines are from ref[4].

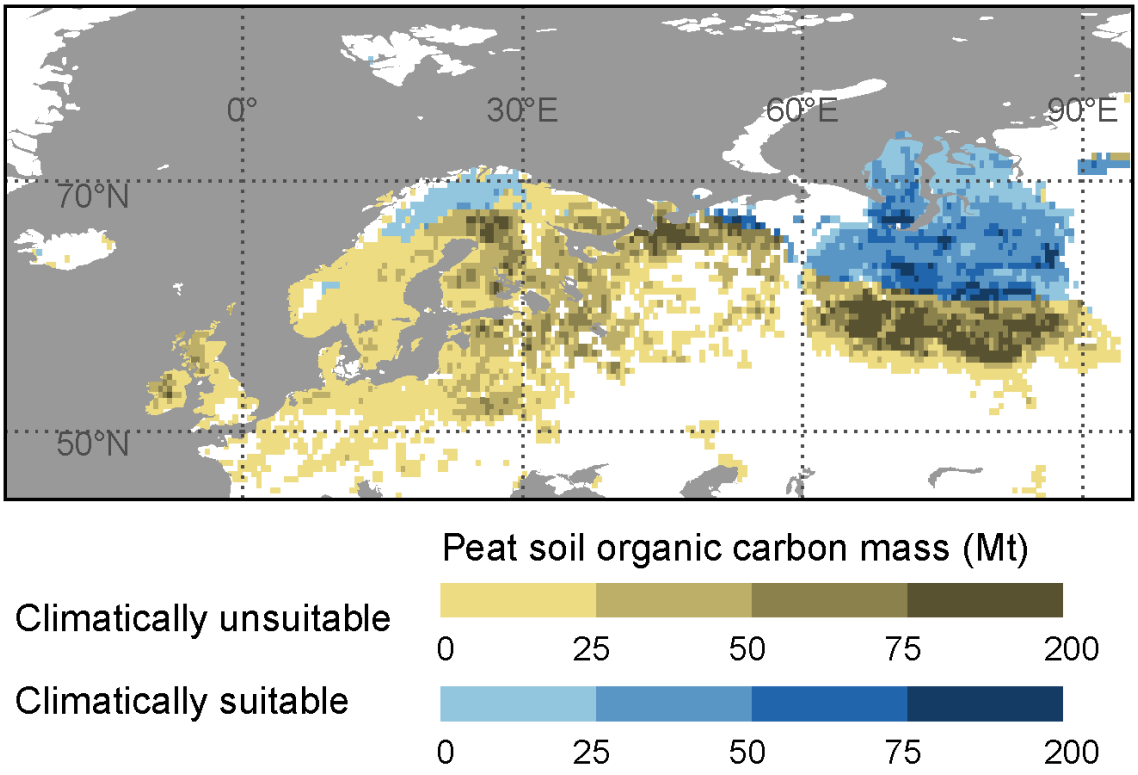

Figure S2 – The distribution of gridded peat soil organic carbon mass (Mt), based on recent soil maps[3,5] (see methods for details) and coloured according to the predicted presence and absence of suitable climatic conditions for permafrost peatlands. Map outlines are from ref[4].

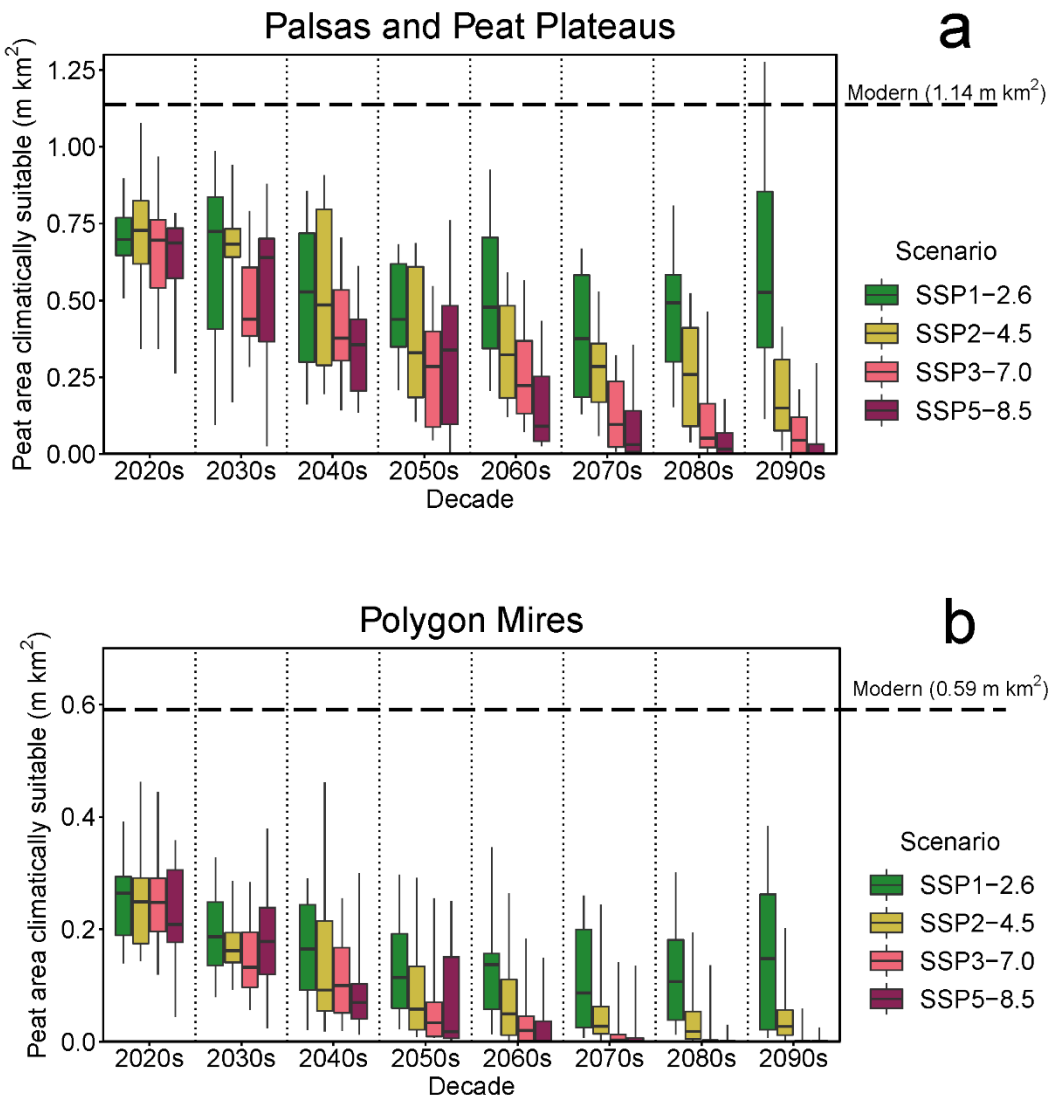

Figure S3 – Comparisons of the total peatland area (m km^2) that is within the suitable climate envelopes for peatland permafrost in Europe and Western Siberia under four CMIP6 emission scenarios. Decadal time series showing for SSP1-2.6, SSP2-4.5, SSP3-7.0 and SSP5-8.5 the total peatland area in Europe and Western Siberia that is: a) within the suitable climate envelope for palsas/peat plateaus; and b) within the suitable climate envelope for polygon mires. Whiskers indicate the full range of values from the 12 CMIP6 models in our ensemble, lower hinges indicate the 25th percentiles, upper hinges indicate the 75th percentiles, and centre lines indicate median values. Dashed lines represent the total peatland area that is within the respective suitable climate envelopes during the modern baseline period (1961–1990).

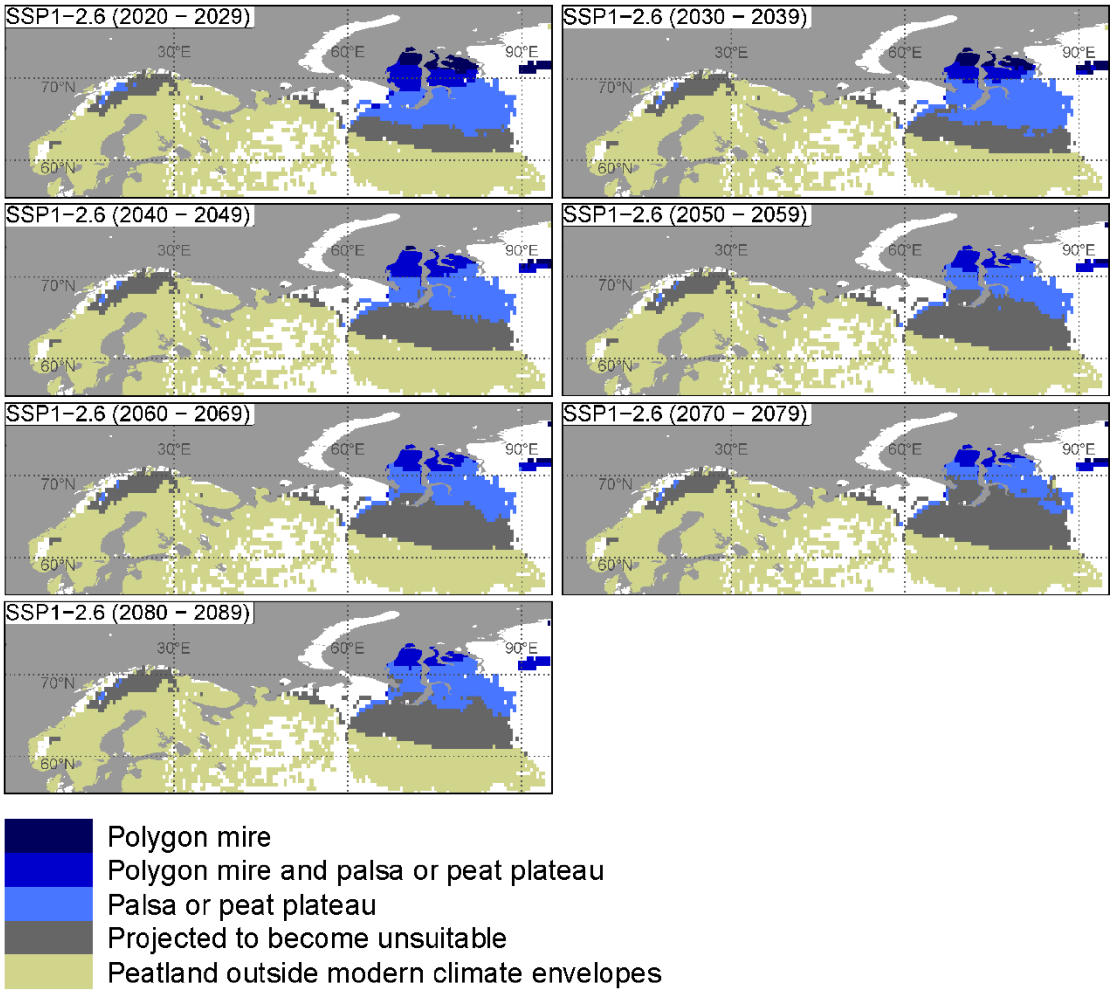

Figure S4 – Projected decadal distributions of the suitable climate envelopes for palsas/peat plateaus and polygon mires in Europe and Western Siberia under SSP1-2.6 (strong climate change mitigation) from 2020–2029 to 2080–2089. Map outlines are from ref[4].

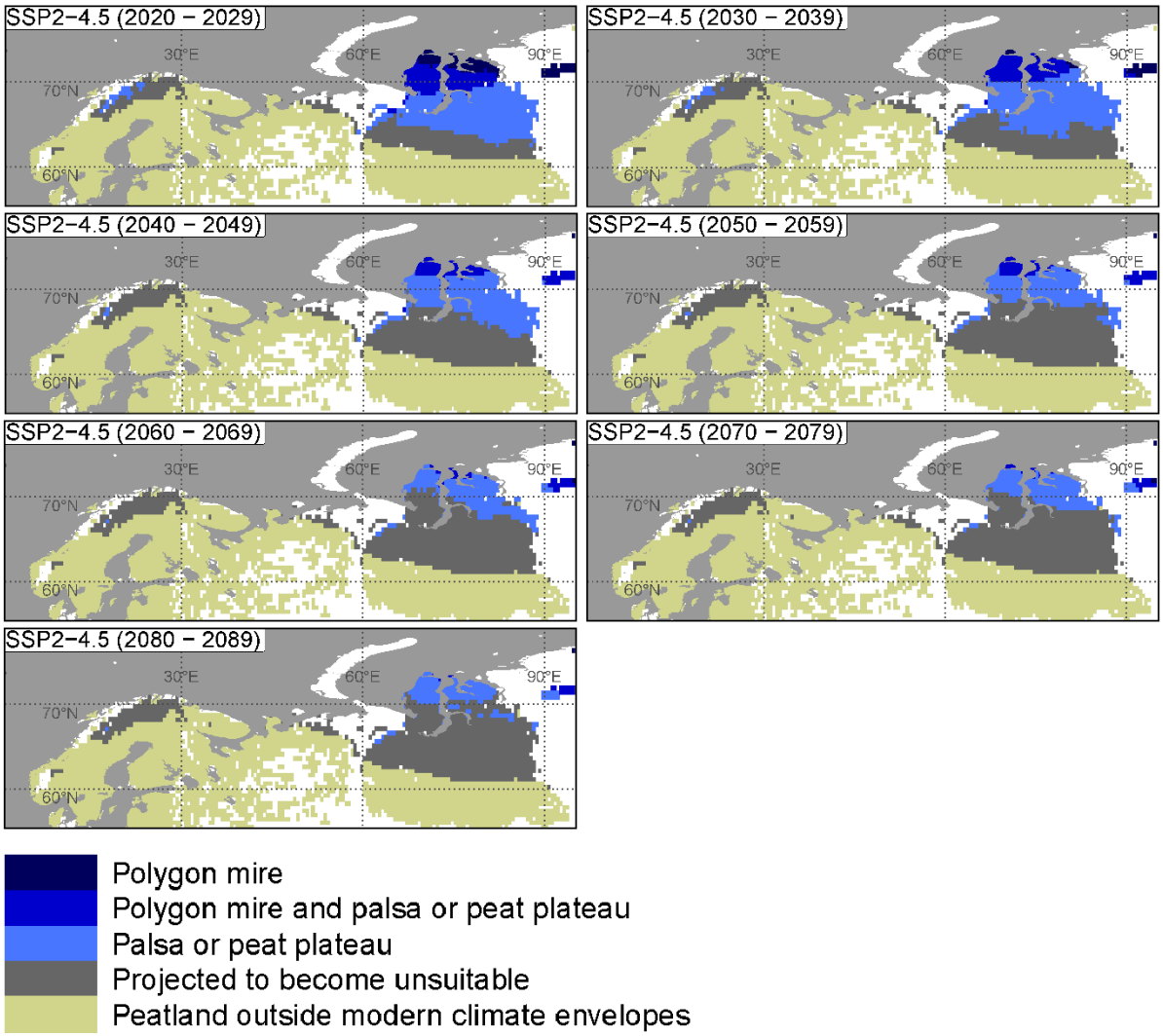

Figure S5 – Projected decadal distributions of the suitable climate envelopes for palsas/peat plateaus and polygon mires in Europe and Western Siberia under SSP2-4.5 (moderate mitigation) from 2020–2029 to 2080–2089. Map outlines are from ref[4].

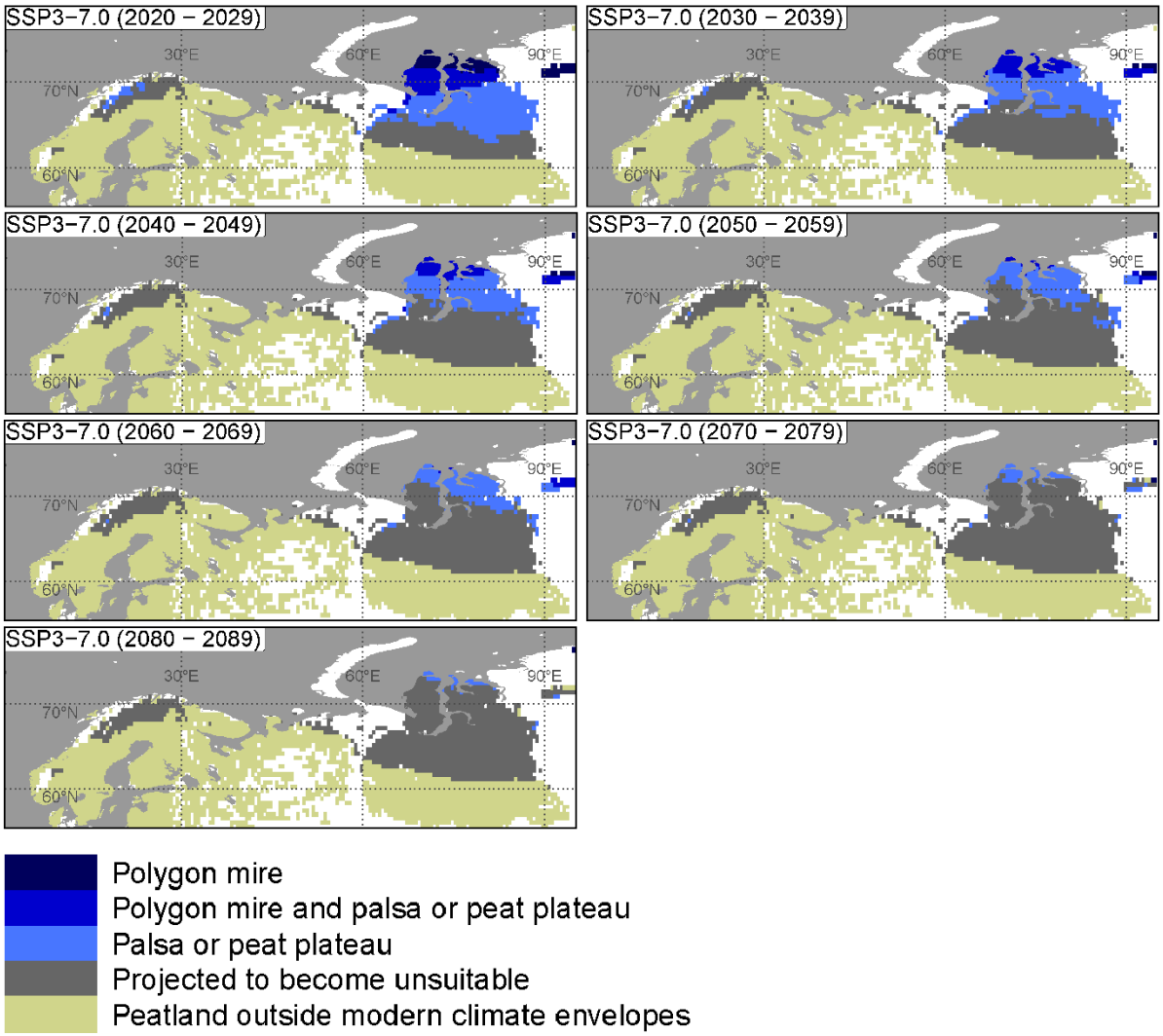

Figure S6 – Projected decadal distributions of the suitable climate envelopes for palsas/peat plateaus and polygon mires in Europe and Western Siberia under SSP3-7.0 (no mitigation baseline) from 2020–2029 to 2080–2089. Map outlines are from ref[4].

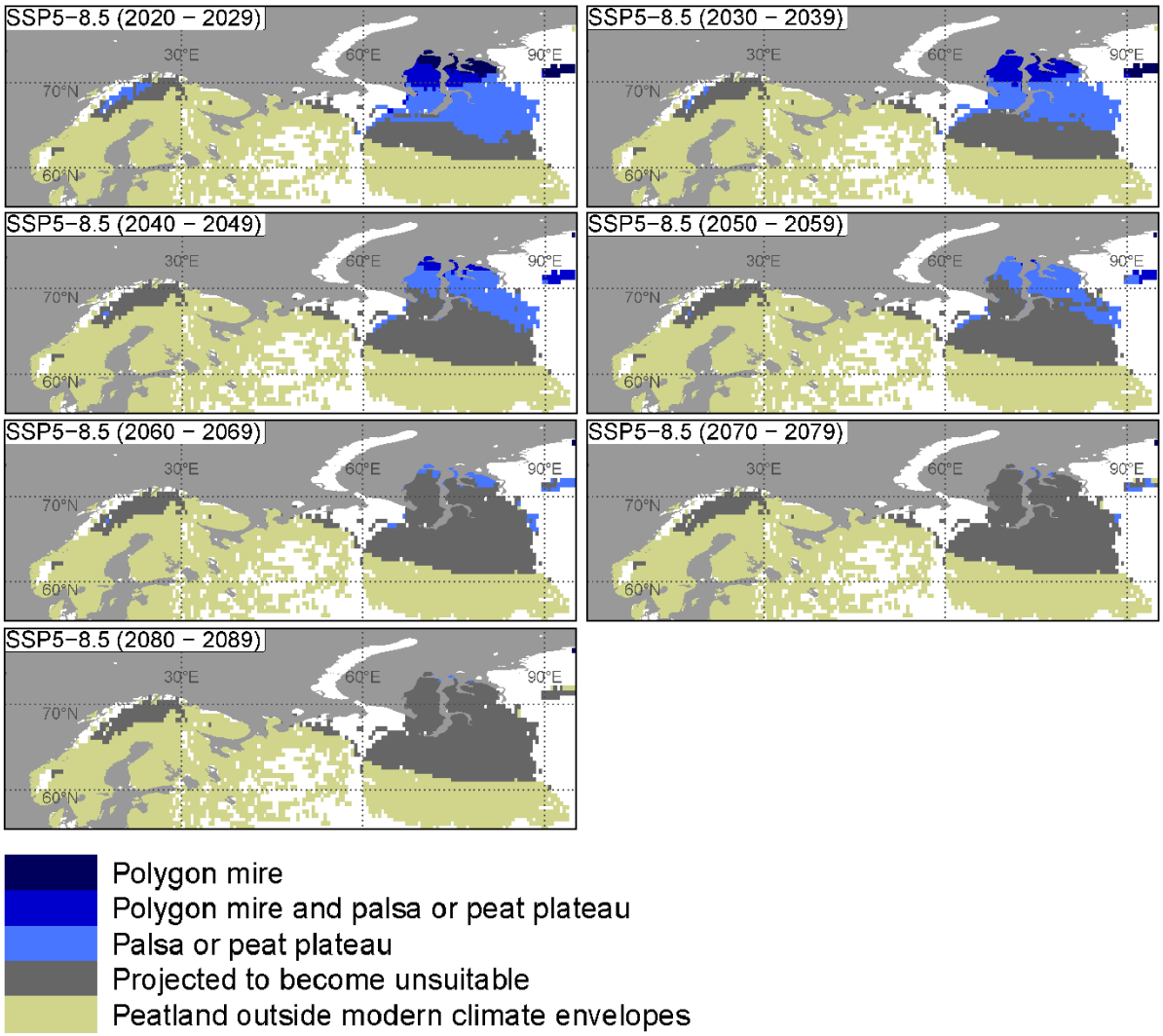

Figure S7 – Projected decadal distributions of the suitable climate envelopes for palsas/peat plateaus and polygon mires in Europe and Western Siberia under SSP5-8.5 (no mitigation, worst-case) from 2020–2029 to 2080–2089. Map outlines are from ref[4].

Reference List

1 Meehl, G. A. *et al.* Context for interpreting equilibrium climate sensitivity and transient climate response from the CMIP6 Earth system models. *Science Advances* **6**, eaba1981 (2020).

2 Menard, S. Standards for Standardized Logistic Regression Coefficients. *Social Forces* **89**, 1409-1428 (2011).

3 Hugelius, G. *et al.* Large stocks of peatland carbon and nitrogen are vulnerable to permafrost thaw. *Proc Natl Acad Sci U S A* **117**, 20438-20446, doi:10.1073/pnas.1916387117 (2020).

4 Brownrigg, R. *mapdata: Extra Map Databases* https://CRAN.R-project.org/package=mapdata (2018).

5 Hugelius, G. *et al.* Maps of northern peatland extent, depth, carbon storage and nitrogen storage. Dataset version 1.0. *Bolin Centre Database*. doi.org/10.17043/hugelius-2020 (2020).